The Newport Line off Oregon – Studies in the North East Pacific

Adriana Huyer*, Patricia A. Wheeler, P. Ted Strub, Robert L. Smith,
Ricardo Letelier and P. Michael Kosro

*College of Oceanic and Atmospheric Sciences
Ocean Admin Bldg 104
Oregon State University, Corvallis OR 97331-5503
541-737-2108, Fax: 541-737-2064
ahuyer@coas.oregonstate.edu

Abstract

The Newport Hydrographic (NH) Line along 44.65°N off central Oregon was sampled seasonally during two epochs: 1961-1971 through the TENOC program and 1997-2003 through the GLOBEC Northeast Pacific Long Term Observations Program (LTOP); some observations are available for 2004 and 2005. During TENOC, the line extended 305 km offshore to 128°W, with stations 18 km apart over the continental shelf and 36 km offshore. During LTOP, the line was shorter (to 126°W) with closer station spacing over the continental shelf (9 km apart) and slope (18 km apart). LTOP cruises included biochemical sampling and underway current measurements. During both TENOC and LTOP, the seasonal cycle is very strong (accounting for >50% of the variance in surface layer properties), with rapid transitions in spring and fall. The summer regime is subject to coastal upwelling driven by southward winds, equatorward surface currents, and advection of low salinity waters from the Columbia River. The winter regime off Newport is subject to coastal downwelling and poleward surface currents driven by northeastward winds. Comparison between TENOC and LTOP summer regimes shows the near-surface layer (0-100 m) at most locations is significantly warmer and fresher during LTOP than TENOC, and steric heights over the continental margin are significantly higher. Comparison of LTOP and TENOC winters shows that average differences at most locations were not statistically significant, but that the variance of steric height and shelf-break temperatures was significantly higher during LTOP than TENOC. Interannual variability of climate indices is also stronger during LTOP, which included a rare Subarctic invasion in 2002 as well as the strong 1997-98 El Niño. During both TENOC and LTOP, interannual variability of steric height is closely related to the

El Niño/La Niña cycle; interannual variations in water properties such as halocline temperature have somewhat longer time scales. Nutrient concentrations and nitrate-to-phospate ratios of upwelling-source waters vary inversely with halocline temperature. Both reflect alongshore advection by coastal currents: southward currents bring cool, nitrate-rich waters in summer (especially during the Subarctic invasion), and northward currents bring relatively warm, nitrate-poor waters to the NH line in winter (especially during El Niño). Seasonal and interannual variations in the nutrient level of upwelling source water are reflected in time-series of vertically-integrated chlorophyll over the LTOP survey region (about 150 km by 300 km). Seasonal variations in chlorophyll and currents are congruent with seasonal variations in copepod biomass and diversity. We were not successful in establishing a clear connection between chlorophyll levels and interannual variations in copepod biomass or diversity, nor in explaining the large decrease in the survival rate of coho salmon between TENOC (6%) and LTOP (3%).

Keywords: Climate change; time series; hydrography; upwelling; coastal ocean; California Current.

Regional Terms: USA, Oregon, Newport.

Contents

1. Introduction

Newport Line oceanographic sampling started later and has ventured less far offshore than CalCOFI and Line-P, its sisters to the South and North. Its origin was not a response to an immediate societal need (the collapse of a fishery or the need for an ocean weather station) but rather to "newly available funds" seeking a use. In 1958 the Office of Naval Research prepared the "TENOC" report (The Next Ten Years of Oceanography) as a plan to increase research funding and ship construction. Wayne Burt at Oregon State College responded immediately, obtained funds to construct the R/V ACONA (the first vessel designed and constructed for oceanographic research in the US since World War II) and started oceanographic sampling of Oregon coastal waters. Coastal oceanography was an obvious task for a new oceanographic institution with an 80-foot vessel. As Wayne V. Burt (cited by Burt and Ludwig, 1998) wrote in 1958: "In general, coastal oceanography out to the 1000 fathom depth has been neglected. This is particularly true of our west coast … Oregon State College is in a unique position to carry out a research program of vital importance to the nation."

Although sampling over the continental shelf off Newport had started in 1958 using US Coast Guard vessels stationed at Newport, we take 1961 as the start of the Newport Line time series. On 26 June 1961, the newly commissioned R/V ACONA began a survey along latitude 44°39.1′ N out to 165 nautical miles making hydrographic casts to 1000 m with Nansen bottles and reversing thermometers. This line (Fig. 1) came to be known as the Newport Hydrographic Line (NH); sampling along this latitude, and at the same stations, continued almost bi-monthly for 11 years. We refer to the 1961-1971 period of regular sampling as the TENOC period. The most complete data for the TENOC period are the physical oceanographic data from hydrographic casts (temperature and salinity vs. depth); biological and chemical observations were added as sampling techniques evolved.

Funding for TENOC ended by 1972 and interest in "monitoring" time-series was eclipsed by process studies. However, the TENOC decade of Newport Line observations encouraged later investigators to include observations on the NH line as part of process studies in the region. The recognition that interdecadal fluctuations in the populations of salmon and other species seem to coincide with physical and atmospheric conditions

(Fig. 2), especially in the coastal Gulf of Alaska and California Current systems (e.g., Francis and Hare, 1994), helped shape a GLOBEC (Global Ocean Ecosystems Dynamics) study in the region.

Part of the GLOBEC study was a Long Term Observational Program (LTOP), which resumed seasonal sampling on the Newport Line from 1997 to 2003. Some other studies occasionally sampled the Newport Line between 2000 and 2005 and these data are included in our analyses. We refer to the 1997-2005 period of sampling as the LTOP period. The Newport Line sampling during LTOP differed from that during TENOC: biological and chemical sampling were included as an integral part of the sampling protocol during LTOP, and the oceanography over the continental margin was emphasized by adding stations over the shelf to make maximum station spacing 5 nautical miles (*vs*. 10 during TENOC), but ending the line 85 nautical miles offshore (Fig. 1). The physical oceanographic data during LTOP were acquired with dual sensor CTDs and a shipborne ADCP was routinely employed. As discussed in the Appendix, we are confident that these data can be directly compared to the data obtained with reversing thermometers and Nansen bottles during TENOC.

The resumption of regular seasonal sampling along the Newport Line in LTOP motivated us to assemble and reanalyze the TENOC hydrographic data to provide a basis for comparison with later observations (Smith et al., 2001). Some LTOP sections have already been compared with the TENOC seasonal averages (Smith et al., 2001; Huyer et al., 2002; Freeland et al., 2003). In this paper, we determine the strength of the seasonal cycles and provide seasonal comparisons of mean physical oceanographic conditions during LTOP and TENOC periods. The effect of the large interannual variability in the physical environment during LTOP is investigated using the LTOP biological and chemical data simultaneously collected.

Some major characteristics of the Newport Line are obvious in the plots of the surface (10 m) temperature and salinity from TENOC and LTOP (Fig. 3a and 3b; the plots show the locations of the Newport Line data, including observations made as part of process studies). The seasonal cycle is very strong, and has rapid transitions in spring and fall with relatively persistent regimes in summer and winter. In summer the water over the continental shelf is cooler and more saline as a result of coastal upwelling while the

southward advection of the Columbia River plume provides a sharp contrast between "offshore" and "coastal" waters in the surface layer. In winter the Columbia River plume is directed northward by the winds, away from the Newport Line, but coastal runoff and downwelling freshens inshore coastal waters. El Niño of 1997-8 is especially apparent in the 10 m temperature.

2. Seasonal Variation of Temperature, Salinity and Steric Height

The seasonal cycle accounts for much of the temporal variability along the NH line. Sources of seasonal forcing include the air-sea heat flux (heating in summer, cooling in winter), alongshore wind stress (upwelling-favorable, southward in summer; northward in winter), advection of diluted Columbia River discharge (southward and offshore from the mouth in summer, northward in winter), and coastal runoff from small rivers and streams (neglible in summer, appreciable in winter). Landry et al. (1989) used this data set to compare summer and winter regimes of the Oregon continental shelf. Smith et al. (2001) used block-averaging of the TENOC data to obtain historical averages of temperature, salinity, steric height, and geostrophic velocity for three seasons: summer, late autumn, and winter (22 June to 31 Aug., 1 Nov. to 21 Dec., and 1 Jan. to 29 Feb., respectively), and for two transition months (April and September). Here we isolate the seasonal cycle by fitting annual and semiannual harmonics to the data.

Seasonal harmonics were calculated separately for TENOC and LTOP because not all stations were sampled in both periods; within each period, the fit was determined independently for each station. The distribution of data through the year is better for TENOC than LTOP (see dots in Figs. 4, 6).

2.1 *Seasonal Variation in the Surface Layer*

The surface-layer temperature (Fig. 4a) varies strongly with season, especially in the offshore region, where the two-harmonic fit accounts for 90% of the variance. Offshore surface temperatures reach their maximum at the end of August and their minimum in March, as expected from the climatological air-sea heat flux (Nelson and Husby, 1983). Inshore, however, the seasonal temperature minimum occurs in summer (July) when coastal upwelling is strongest, and its maximum occurs in autumn (late

October) after seasonal upwelling has ceased. The seasonal cycle inshore accounts for only about 50% of the surface temperature variance, probably because the intensity of coastal upwelling varies on time scales of several days (Halpern, 1976; Huyer, 1983).

The surface-layer salinity (Fig. 4b) also varies strongly with season, especially over the inner shelf and offshore between 125° and 126.5°W, where the two-harmonic fit accounts for about 75% of the variance. Lowest salinities (<31.5 psu) occur between 124.5° and 126.0°W in late spring and summer (May to July) when Columbia River discharge is high (Sherwood et al., 1990), surface currents are predominantly southward (Reid and Mantyla, 1976; Hickey, 1998; Kosro, 2005) and surface Ekman transport is offshore. The low-salinity Columbia River plume waters (S < 32.5 psu, Barnes et al., 1972) are first seen over the outer shelf (in Mar.-Apr.) and migrate slowly offshore as the upwelling season progresses until their seasonal disappearance from the NH-line in late September. Offshore surface salinities reach their seasonal peak in late winter (Feb. - March) while inshore salinities are highest during the summer upwelling season. Inshore surface salinities are lowest in winter (Jan.-Feb.) when there is strong downwelling and coastal rainfall is high (e.g. 28 cm in January at Newport *cf.* 2.5 cm in July; Taylor and Hannan, 1999).

Steric height (geopotential anomaly) of the sea surface is the vertical integral of specific volume anomaly over the layer extending down from the surface to a specified reference surface (we use 500 dbar). A steric height change of 0.1 J/kg corresponds to a 1 cm change in layer thickness, and thus the variations in steric height provide an estimate of variations in sea surface elevation that are due to changes in the density of the underlying water column. Shallow water values of steric height can be estimated by the method of Reid and Mantyla (1976), which yields coastal sea level values that are in good agreement with tide gage data (Huyer, 1977; Huyer et al., 1979). The seasonal range and phase of steric height along the NH line (Fig. 4c) vary strongly with longitude. Over the continental shelf, the minimum falls in summer and the maximum falls in winter. Far offshore (west of 127°W), the minimum occurs in March and the maximum occurs in September; the seasonal range here is similar to the range observed at Station 4 of Line P (Tabata et al, 1986). Over the continental slope (125°W), the zonal gradient of steric height changes sign in autumn (October) and early spring (March/April), indicating

that the surface geostrophic flow is southward in spring and summer and northward in late autumn and winter.

Data from satellite altimeters confirm that the seasonal variation of steric height is a reasonable represention of sea surface elevation. Figure 5a shows the two-harmonic fit of sea level anomaly (SLA) calculated from 13 years (1993-2005) of gridded altimeter data between 44.1°N and 45.1°N, plotted as a function of time-of-year and longitude. As with all altimeter analyses, the temporal mean has been removed from the altimeter data at each spatial point to eliminate the marine geoid, leaving the sea level anomaly (SLA). This also removes the long-term mean onshore-offshore gradient in sea surface height, which consists of a relatively gentle downward slope toward the coast (based on Levitus climatology, as presented in Strub and James [2002]). Inshore of 128°W, the timing and location of seasonal highs and lows in the SLA in Figure 5a are similar to those of the geopotential anomalies in Figure 4. As in the geopotential anomaly (Fig. 4c), there is a sharp gradient in the phase of the seasonal cycle between 125° and 126°W, where both the amplitude and percent variance are small. At 128°W, the offshore end of the NH line during TENOC, the maximum occurs in September and the minimum occurs in March-April; the seasonal range is about 11 cm, compared to 13 cm in steric height (Fig. 4). At 124.3°W, near the coast, the maximum occurs in January and the minimum occurs in June-July; the range is about 14-15 cm, somewhat smaller than the 20 cm range in steric height (Fig. 4). The discrepancy may be due to problems with atmospheric corrections in regions near the coast, especially errors due to atmospheric water vapor, which is not well resolved by the onboard radiometer in regions near land.

Zonal gradients of sea surface elevation are directly proportional to meridional geostrophic velocities. To reveal these gradients clearly in the altimeter data, the spatial mean of sea surface height was removed at each time step (thus removing the spatially-uniform component of any seasonal variation, which is dominant offshore), and two-harmonic fits were recalculated. The result (Fig. 5b) no longer has an abrupt gradient in phase (nor a minimum in percent variance) between 125° and 126°W. Instead, it clearly shows the zonal gradients and associated geostrophic flow. Near the coast at 125°W, meridional surface velocities are northward during autumn and winter (November – March) and southward during spring and summer (May – September), similar to the sense of

velocities derived from the geopotential anomaly (Fig. 4c). A band of negative gradient (southward current, centered on the 0 cm contour in Fig. 5b) begins near the coast (124.5°W) in April-May, and migrates offshore to reach 127°W in mid-October. A band of positive gradient (northward current, centered on the 1 cm contour in Fig. 5b) begins near the coast in October-November and migrates offshore to reach 127°W at the end of May. The ridge of high SLA is at approximately 124.5°W in January-March and at 128°W in mid-September. The inferred propagation speed for the ridge is about 1.4 cm s^{-1}. Such westward propagation of sea level signals seems to be ubiquitous and can be interpreted as a manifestation of baroclinic Rossby waves (Fu, 2004; Chelton and Schlax, 1996). The theoretical phase speed for the first-mode baroclinic Rossby wave at 45°N is about 1 cm s^{-1} (Fig. 5 in Chelton and Schlax, 1996), which is slightly less than the propagation speed observed here. Chelton and Schlax (1996) also found observed propagation speeds at mid-latitudes to be greater than the theoretical values, by a factor of 1.5-2 in the North Pacific.

2.2 *Seasonal Variation at 150 m*

The seasonal variation of temperature and salinity at 150 m (Fig. 6a,b) show that the effects of coastal upwelling and downwelling penetrate down to 150 m, but the effects of surface heating and freshwater runoff from the Columbia River and coastal streams do not. At the shelf-break (124.6°W, NH-25), low summer temperatures and high summer salinity values coincide with strongest seasonal upwelling, and high winter temperatures and low winter salinities coincide with strongest downwelling. Geopotential anomaly at the shelf-break is lowest in spring and highest in winter (Fig. 6c). Data from the full length of the NH-line (sampled during TENOC with very good seasonal coverage) suggest that this subsurface response to seasonal upwelling (low T, high S, low geopotential anomaly) propagates offshore at a rate of about 1 km per day, about the same rate as the propagation of sea level anomaly extrema and gradients (Fig. 5b); its amplitude decays appreciably between the shelf-break and 126°W.

Over the continental slope (inshore of 125.3°W), the zonal gradient of the geopotential anomaly at 150m (Fig. 6c) is negative from March through July (indicating southward geostrophic flow), and positive from August through January (indicating northward flow). In late summer and early fall (August through October), the northward

geostrophic flow at 150 m along the continental slope opposes the overlying southward current at the surface (Figs. 4c, 5). This northward flow is the poleward undercurrent of the California Current system, which extensive summer shipborne ADCP (Acoustic Doppler Current Profiler) surveys have shown to be present along most of the mid-latitude (33° to 51°N) eastern boundary of the North Pacific, centered about 25 km seaward of the shelf break at depths between 125 and 325 m (Pierce et al., 2000). Extensive surveys have not been done in other seasons, but our data suggest a strong seasonal variation.

Low salinity and high steric height values west of 127°W suggest southward advection of Subarctic water in summer and autumn; this is consistent with June and September mean geostrophic velocities on Line P (Whitney and Freeland, 1999, their Fig. 5).

2.3 *Seasonal Variation of the 33.0 Isohaline*

As noted by Wheeler et al. (2003), the inshore portion of the permant halocline provides much of the water upwelling to the surface along the coast during summer. This halocline has a salinity range of 32.8 to 33.8 psu, and in summer it typically lies at mid-depth over the mid- and outer continental shelf; its upper portion lies within the mid-depth layer of onshore return flow described by Huyer (1976). To represent the upper halocline, we choose the 33.0 psu isohaline. The TENOC seasonal mean sections in Smith et al. (2001) show that the 33.0 psu isohaline lies at a depth of about 80 m in winter and slopes up to the surface layer in summer. This isohaline lies in or near the permanent pycnocline (25.5 to 26.5 kg m^{-3}) which forms the coastal upwelling front in spring and summer (Mooers et al., 1976). In winter it often intersects the shelf bottom, and in summer it often intersects the sea surface. Figure 7a shows the depth of the S = 33 psu surface is nearly uniform in winter (Jan. and Feb.). During spring and summer, the inshore end rises, while the far offshore portion (west of 126°W) deepens slightly. During autumn, the inshore end deepens, while the offshore portion shoals.

Temperature variations on an isohaline within the strongly stratified halocline represent water-mass changes and usually reflect advection by the flow. A very shallow isohaline could also be affected by seasonal heating, but we see little evidence of this on

the 33.0 psu surface except where its depth is <20 m. The shelf-break T-S diagrams presented by Smith et al. (2001, their Fig. 11) show the temperature at 33.0 psu is highest in fall and winter, and lowest in summer. Figure 7 shows summer minimum temperatures occur close inshore, with values <8.2°C over the mid-shelf (NH-15) in both TENOC and LTOP. This summer minimum is colder than and isolated from cool waters offshore, and must therefore reflect advection of cool subarctic water from the north. The location, small zonal extent, and duration of the summer minimum indicate this advection occurs predominantly through the baroclinic jet associated with coastal upwelling. Thus the "cool ribbon" observed in 1972 (Huyer and Smith, 1974) was not an isolated event, but rather represents a regular seasonal phenomenon. During late summer and fall, the temperature minimum migrates slowly offshore while its intensity decreases.

During late fall and winter, the temperature on this isohaline increases gradually with time in the region inshore of 126°W as northward geostrophic flow (Fig. 4c, 6c) advects warmer water northward along the coast.

3. Comparison of TENOC and LTOP Regimes

Interdecadal climate change is often cited as an important factor in the decline and recovery of salmon fisheries along the Pacific Northwest coast of the United States (*e.g.*, Mantua et al, 1997; Koslow et al., 2002). Sampling of Line P in the Gulf of Alaska (Fig. 1) and the CalCOFI grid off southern California have provided evidence of interdecadal or long-term change in both of these regions (Whitney and Freeland, 1999; McGowan et al., 1998). It is therefore of interest to determine whether the regime along the NH line changed significantly between the TENOC and LTOP epochs whose midpoints are separated by 35 years.

Close inspection of Figures 4, 6 and 7 suggests there may be important differences between the seasonal cycles calculated from the TENOC and LTOP data sets. At NH-45, and over the continental slope in general, the seasonal maximum 10 m temperature is >1°C higher during LTOP than TENOC, the minimum 10 m salinity is >0.5 psu lower, and the steric height maximum is >0.2 J kg^{-1} higher. It is, however, difficult to know whether differences between these seasonal cycles are statistically significant, given the different sampling schemes in the two periods, and the natural

variability on other time scales. We therefore use a different approach to determine whether there have been significant changes along the NH line between the TENOC and LTOP periods.

Our comparison of the two epochs is limited to two seasons, summer and winter, because conditions within each of these seasons are relatively persistent and because these seasons were adequately sampled during both programs. The summer regime has coastal upwelling driven by southward winds, equatorward surface currents, and advection of low salinity waters from the Columbia River. The winter regime off Newport has strong coastal downwelling, and poleward surface currents driven by northeastward winds. During TENOC, the NH line was sampled in eleven summers and ten winters (1961-1971). During LTOP it was sampled in nine summers (1997-2005) and six winters (1998-2003); due to stormy weather, the February 1999 section is incomplete (only the shelf and upper slope stations were sampled). For each season, we compare both means and variances. TENOC statistics were calculated from all available data (see Table 2 of Smith et al., 2001); for LTOP statistics, we used only one section per season per year.

3.1 *Summer Temperature and Salinity*

The LTOP summer temperature average (Fig. 8b) is generally similar to the TENOC summer average (Fig. 8a) calculated by Smith et al. (2001). Both show very warm (>16°C) surface water offshore and very cool (about 10°C) surface water inshore. Both also show isotherms in the upper 300 m tilting up toward the coast. Careful examination reveals that the average surface temperatures are warmer, and the average isotherms above 6.5°C are deeper, during LTOP than TENOC.

The TENOC and LTOP summer salinity averages (Fig. 8d,e) are generally similar. Both show minimum surface salinities < 31 psu near NH-45, 83 km from shore. This thin lens of very fresh water is associated with the Columbia River Plume which usually tends southwest from Astoria in summer (Barnes et al., 1972; Pak et al., 1970). Both also show subsurface isohalines at depths above 200 m rising steeply toward the coast, and inshore surface salinities of about 33.2 psu. Close inspection reveals that the

summer surface layer is generally fresher and that both the surface salinity minimum and the surface salinity front lie closer to shore during LTOP than TENOC.

3.1.1 *Summer Differences: LTOP Minus TENOC*

Differences between LTOP and TENOC summer average temperature and salinity were calculated for the standard sampling depths at the seven locations that were sampled routinely during the 1961-1971 period (i.e., 0, 10, 20, 30, 50, 75, 100, 150, 200, 250, 300, 400, 500, 600, 700, 800 and 1000 m at NH-5, NH-15, NH-25, NH-35, NH-45, NH-65 and NH-85). We use the t-test as outlined by Snedecor and Cochran (1967, Section 4.10) to estimate the statistical significance and confidence intervals of these differences.

Temperature differences between LTOP and TENOC (Fig. 8c) are positive at all locations above 500 m. Greatest differences (0.5 to 2°C) occur in the seasonal thermocline (at temperatures of 10-15°C and depths <50 m); these are significant at the 95% level at all but the most offshore station. Smaller temperature differences (0.2 to 0.5°C) are also significant in a subsurface area centered at a depth of 200 m, 100 km from shore. Thus there has been significant warming between the 1961-71 and 1997-2005 epochs in the seasonal thermocline and in a region offshore of the shelf-break. The rate of warming is a strong function of depth and location; at 200 m, 120 km offshore, the rate is about 1°C per century, about half the value reported for Ocean Station Papa at 50°N, 145°W (Whitney and Freeland (1999).

Salinity differences (Fig. 8f) are mostly negative, except at depths of 100-250 m and in the most offshore portion of the surface layer. Differences are especially large (>0.4 psu) on the inshore side of the Columbia River Plume (above 30 m, 30-70 km from shore). Smaller salinity differences (~0.2 psu) in a tongue lying approximately along the 33.0 psu contour within the permanent halocline are also significant; these indicate the halocline lies deeper during LTOP than TENOC. Reduced salinities in both of these regions cannot be the result of a change in the strength of local summer upwelling, which is about the same during LTOP and TENOC (Table 1, Fig. 2). They could, however, result from weaker upwelling in spring: Table 1 shows the average offshore component of surface Ekman transport was 40% less during LTOP than TENOC. Recent process

studies have shown that the position of the coastal upwelling front is strongly affected by the strength of the upwelling-favorable wind stress (Austin and Barth, 2002). Recent radar observations of surface currents indicate that the coastal jet migrates gradually offshore during the upwelling season in response to continuing upwelling-favorable wind stress (Kosro, 2005). Thus weaker spring-season coastal upwelling during LTOP might explain the greater depth of the halocline over the shelf and shelf-break during LTOP than TENOC.

At depths below 400 m, LTOP salinity values are significantly lower than those in the TENOC period, but the difference is very small (~0.03 psu); the rate of this deep freshening (about 0.1 psu per century) is similar to the rate observed at Ocean Station Papa (Whitney and Freeland, 1999).

3.1.3 *Summer Variance Ratios: LTOP/TENOC*

Standard errors of the mean summer temperature and salinity tend to be larger during LTOP than TENOC, suggesting that interannual variability might have increased (e.g., in response to the strong 1997-98 El Niño, Fig 2). A 2-sided F-test (Snedecor and Cochran, 1967, Section 4.15) indicates that values of the variance ratio need to exceed 2.64 to be significant (for P>90%, with 8 and 15 degrees of freedom). Values greater than this threshold occur in only a few locations, different for each variable, and thus we reject the hypothesis that interannual variability of the summer season is stronger during LTOP than TENOC.

3.2 ***Winter Temperature and Salinity***

Both TENOC and LTOP winter averages (Fig. 9a,b) show isotherms sloping generally down to the east along the entire 160-km section; warmest surface waters occur over the continental shelf. The LTOP winter average (Fig. 9b) includes data from the 1997-98 El Niño (Huyer et al., 2002). Nevertheless, average shelf temperatures are only about 0.5°C higher during LTOP than TENOC, and the difference is not significant at the 95% level. At other locations, TENOC and LTOP winter average temperatures are very similar, with LTOP only slightly warmer than TENOC.

TENOC and LTOP winter salinity averages (Fig. 9e,f) are also very similar to each other, with no significant differences. Both show the permanent halocline (32.6-33.8 psu) lying very nearly level between 50 and 150 m. Both also show the inshore lens of fresh water at the surface that is due to coastal trapping of winter runoff by onshore Ekman transport. In both averages, mean isohalines (Fig. 9e,f) tend to intersect mean isotherms (Fig. 9a,b), indicating significant water mass gradients: inshore waters tend to be warmer and more saline than offshore water of the same density.

3.2.1 *Winter Differences: LTOP Minus TENOC*

Winter temperatures at most depths are slightly higher during LTOP than TENOC, with largest differences in the surface layer (Fig. 9c); these differences are not significant even at the 90% level. As in summer, positive salinity differences are observed in the layer with salinities of 33.9 to 34.0 psu (North Pacific Intermediate Water; Talley, 1993), Negative salinity differences at depths between 50 and 150 m (Fig. 9g) suggest the halocline was slightly deeper or fresher during LTOP than TENOC, as it was in summer (Fig. 8f). Salinity differences over the inner shelf are positive, suggesting less winter runoff LTOP than TENOC. Because of high interannual variability in winter, none of the these salinity differences are significant even at the 90% level.

3.2.2 *Winter Variance Ratios: LTOP/TENOC*

The ratio of temperature variance (LTOP/TENOC) has values >3 over the shelf-break and outer shelf (Fig. 9c), indicating that LTOP has significantly greater variance than TENOC (P>90%, 2-sided F-test with 5 and 15 degrees of freedom). The El Niño signature in Oregon waters tends to peak in winter (Huyer and Smith, 1985; Huyer et al., 2002); thus the increase in year-to-year variability during LTOP results partly from the strong 1997-98 El Niño that occurred during LTOP. Table 1 shows that winter downwelling, equatorial forcing, and the Pacific Decadal Oscillation were all more variable during LTOP than TENOC.

Values of the salinity variance ratio (LTOP/TENOC) exceed the 90% significance threshold in only a few isolated locations (Fig. 9h); these may not be significant.

3.3 *Nonseasonal Changes in Temperature and Salinity*

The comparison of average summer salinities (Fig. 8) indicates that offshore subsurface waters (depths > 400 m) are significantly fresher during LTOP than TENOC, though the salinity difference is small. At this depth and location, we would expect little or no seasonal variation, and thus we pooled all of the available data from NH-85, the most offshore station sampled in both epochs. For each standard depth sampled during both epochs, we calculated the mean difference and corresponding 95% confidence interval (Fig. 10).

As expected, the confidence intervals are very large in the upper 150 m, where seasonal variations are important. Nevertheless, we find significant net warming (Fig. 10a) in the upper half of this layer. Rates (based on the 35 years between mid-points of LTOP and TENOC) decrease with depth from about 3°C per century at 10 m to about 1°C per century at 75 m. Although the net reduction in salinity is not significant at depths above 150 m (Fig. 10b), it combines with the temperature increase to yield a significant reduction in density at depths between 50 and 100 m (Fig. 10c). The associated increase in stratification may be important to the biology. The layer between 175 and 275 m is both warmer and saltier during LTOP than TENOC; the rate of change is about 0.4°C per century for temperature and 0.3 psu per century for salinity (Fig. 10); the combination yields no appreciable change in the density of this layer (Fig. 10c). The layer between 300 and 500 m is significantly warmer, while salinity is unchanged. Between 500 and 900m, LTOP and TENOC temperatures are the same, though salinity is reduced (at a rate of about 0.3 psu per century).

This layered structure of the LTOP-minus-TENOC differences generally resembles the profile of long-term trends estimated for OSP (50°N, 125°W) by Whitney and Freeland (1999), though details differ. Both show warming throughout the upper 1000 m, but the depth of peak warming is much shallower on the NH line (<50 m) than at OSP (about 200 m). Both show freshening of the surface layer above and within the permanent halocline (S <32.8 psu) and in the deep water below about 300 m. Both show a thin layer in which both temperature and salinity are increasing while density remains about the same. The salinity range (33.9 to 34.0 psu) of this layer indicates it lies near the

core of North Pacific Intermediate Water (Reid, 1965; Talley, 1993), which originates in the far northwest Pacific Ocean and spreads eastward throughout the North Pacific (Talley, 1993). The change we see in the properties of this layer is likely to reflect regional changes in the advection and diffusion in the eastern boundary region of this water mass rather than changes in its formation.

Long-term variability has also been observed off Southern California. Bograd and Lynn (2003a) divided 50 years of sampling the CalCOFI grid between Pt. Conception and San Diego into two periods: a 1950-1976 'cool' period and a 1977-1999 'warm' period separated by the 1976-1977 climate shift in the Pacific Ocean (Miller et al., 1994). They found significantly warming (0.2-0.6°C) along both Line 80 off Pt. Conception and Line 90 off San Diego, reaching to depths of at least 250 m near the shelf and to 150-200 m offshore. The combination of these three data sets (i.e., Line P, NH Line, and CalCOFI) suggests that upper waters of the entire California Current have warmed significantly over the last several decades.

3.4 *Steric Height*

The temperature and salinity changes between TENOC and LTOP affect water density, and thus steric height and sea surface elevation. At both Ocean Station P (Whitney and Freeland, 1999) and at NH-85 (Fig. 10), density has decreased over most of the upper 1000 m; this would be consistent with increasing steric height and rising sea level. Such changes are not necessarily uniform over the region, nor steady in time. Figure 11 shows zonal profiles of steric height along the NH line, for individual LTOP sections as well as summer and winter LTOP averages compared to the TENOC seasonal averages.

Each of the nine LTOP summer profiles shows steric height values exceed the TENOC summer average over a large portion of the NH-line (Fig. 11a); at NH-35 and NH-45, the difference is positive each year. At the most inshore stations, individual LTOP steric heights are often near or below the TENOC average, and there is no significant difference between the LTOP and TENOC average.

The winter steric height profiles (Fig. 11b) show much greater year-to-year variability, particularly inshore. The standard deviations of surface elevation increase

shoreward from about 2 cm at NH-85 (offshore) to 10 cm to NH-5 (inshore). Most of the LTOP profiles fall within this large range, but two show even larger deviations. In February 1998, at the peak of the 1997-98 El Nino, steric heights along the entire NH line were significantly above the TENOC average. And in February 2003, after an unusually sustained episode of winter-season coastal upwelling, inshore values of steric height were far below (~2 J kg^{-1}, ~ 20 cm) the TENOC winter average.

3.5 Alongshore Velocity

Geostrophic velocities were calculated for each summer and winter section which included at least two stations with sampling down to 500 m. Horizontal resolution is limited by the station spacing: during TENOC, the spacing was 36 km offshore, and 18 km over the continental shelf; during LTOP, the spacing decreased from 36 km offshore to 18 km over the continental slope, 9 km over the continental shelf outer shelf, and 3 km over the inner shelf. The individual sections were averaged to yield seasonal averages for TENOC and LTOP. Because of the change in station spacing, the summer and winter LTOP averages have much better resolution of the coastal currents than the TENOC averages (shown in Fig. 5b of Huyer et al., 2002). The summer average (Fig. 12a) shows a strongly sheared coastal jet with maximum southward velocity >40 cm s^{-1} at the surface over the continental shelf, and a weak poleward undercurrent (<5 cm s^{-1}) near the shelf-break. The winter average geostrophic velocity (Fig. 12d) is comparatively uniform (poleward at most locations) and weak (<10 cm s^{-1} everywhere except over the inner shelf).

The LTOP sampling protocol included direct measurement of water velocity by means of a shipborne acoustic Doppler current profiler (ADCP). On most cruises we used a 150 kHz RDI transducer and the same sampling and processing protocol described by Kosro (2002). Seasonal averages for measured currents along the NH line were calculated from data for five LTOP winters (1998, 2000-2003) and seven LTOP summers (1997-2003). Eastward (u) and northward (v) components of the measured velocities were first interpolated to a grid with 5 km horizontal and 5 m vertical resolution, and these gridded values were averaged to yield LTOP summer and winter averages.

Comparison of the summer-average measured and geostrophic currents (Fig. 12) shows general similarity, but with some important differences. The ADCP data show that the coastal jet has a significant offshore component, with the equatorward flow tending to follow the orientation of isobaths of the outer continental shelf (see also Kosro, 2005, and Castelao and Barth, 2005). In the core of the coastal jet, geostrophic currents appear to be stronger than measured current, but this is largely because there is significant current shear in the upper 20 m (Huyer et al., 2005; their Fig. 9), which is above the ADCP sampling. The ADCP data also shows that near-bottom currents over the shelf tend to be much weaker than the geostrophic velocities obtained from the extrapolation method of Reid and Mantyla (1976) which *assumes* that there is no horizontal shear at the deepest level sampled by each station pair. Although this interpolation method gives reasonable estimates of near-surface currents (Huyer et al., 2005). it naturally overestimates currents near the bottom, where friction is important (Kurapov et al., 2006); Numerical models also predict weak near-bottom currents (Gan and Allen, 2005). The narrow poleward undercurrent is poorly resolved in the geostrophic velocity field, due partly to the wide (36 km) station spacing; even in the ADCP velocity field it is weak, especially compared to typical undercurrent core velocities observed south of 44°N and north of 48°N (Pierce et al., 2000). The high horizontal resolution of the ADCP data strongly suggests both the southward coastal jet and the poleward undercurrent are narrower than we would infer from the geostrophic velocity field.

The winter-average geostrophic and measured currents (Fig. 12 d,e,f) are also generally similar, but again there are important differences. Both show mostly northward flow. The ADCP data show that the poleward flow over the continental slope and shelf is stronger than we would expect from our estimates of the geostrophic flow. The ADCP currents have an appreciable barotropic component, particularly over the continental slope. Four of the six winter sections show strong northward currents (>20 cm s^{-1}) near the surface over the outer continental shelf and inner slope. The winter averages include the intense poleward currents from the 1997-98 El Niño (Kosro, 2002). The narrow equatorward undercurrent observed that was observed during the 1997-8 El Niño winter (Kosro, 2002) is not seen in multi-year winter averages of either the geostrophic or directly measured velocities, suggesting that it is an anomaly associated with El Niño.

Currents at tidal and higher frequencies contribute to the differences between directly-measured and geostrophic currents, especially over the continental shelf and slope. Diurnal tides are barotropic, with K1 amplitudes of 1 to 5 cm s^{-1}, while semi-diurnal tides (dominantly M2) have a barotropic component of 2 to 4 cm s^{-1}, but can have strong, unsteady baroclinic components, possibly depending on stratification and on the low-frequency current field (Torgrimson and Hickey, 1979; Erofeeva, et al., 2003; Kurapov et al., 2003). Energetic solitons or tidal current bores are observed both in the upper and lower water columns (Curtin and Mooers, 1975; Klymak and Moum, 2003), associated with currents of tens of cm $s.^{-1}$ Nearby moored observations indicate the presence of intermittently energetic inertial currents, with amplitudes up to 30 cm s^{-1} (Anderson et al., 1983). These short-period phenomena have a comparatively small effect on hydrographic variables.

4. Interannual Variability

The seasonal cycles obtained by harmonic fitting (Section 2 above) were used to calculate time series of anomalies for selected variables. To obtain anomalies for the TENOC period, we used the TENOC seasonal cycles; to obtain anomalies for the LTOP period, we used the LTOP seasonal cycles.

Time series of anomalies of steric height (Fig. 13a) show many short-lived perturbations east of 125°W, and a few long-lived perturbations that extend to both ends of the NH-line. In addition, some short-lived, small-scale (one station) perturbations with small amplitude occur throughout our sampling domain; we attribute these to sampling noise due partly to internal waves. Time series of anomalies of dynamic height (geopotential anomaly) at 150 m relative to 500 dbar (Fig. 13b) are similar (correlation coefficient is 0.76 for TENOC and 0.68 for LTOP), except that amplitudes are smaller (regression coefficient is 0.38 TENOC and 0.30 for LTOP). The short-lived perturbations are strongest inshore and decay rapidly with distance from shore over the continental shelf and slope; in this respect they resemble coastal trapped waves (Huyer, 1990). Their duration is not adequately resolved by either the TENOC or LTOP sampling frequency. Some seem to last as long as a few months, while others affect only a single section. They likely represent the rapid response to weather-band (days to weeks)

variations in the alongshore wind stress (e.g., upwelling and downwelling events; Allen, 1980).

Most but not all of the large-scale, long-lived perturbations seem to be associated with the cycle of ENSO (El Niño/Southern Oscillation, i.e., El Niño/La Niña) events in the equatorial Pacific Ocean. There are various indices and classifications of the strength of these events; we show time series of only one index: the Multivariate ENSO Index (Wolter and Timlin, 1998) for which updates are readily available. Smith et al., (2001) note that three periods within TENOC have been classified as significant or weak El Niño events (1965-66, 1963-64, 1969-70) and two have been classified as significant La Niña events (1964 and 1970-71). The MEI (Fig. 13a, Fig. 2) is positive during the three El Niño periods, and strongly negative during the La Niña periods. Persistent positive anomalies in steric height are associated with the El Niño periods and negative anomalies are associated with La Niña. The magnitude of surface elevation anomalies is typically 5-10 cm over the continental margin and <5 cm offshore.

The first half of the LTOP period also shows a tendency for large scale and persistent steric height anomalies to be associated with the ENSO signal (Fig. 13a), as did anomalies of the dynamic height at 150 m (Fig. 13b). The very strong El Niño of 1997-98 raised coastal sea level along the Oregon by as much as 30 cm (Kosro, 2002), and anomalies of >5 cm persisted over the continental shelf for more than six months (Fig. 13a). Sea surface temperature anomalies exceeded 3°C during the autumn and winter of 1997-98 (Kosro, 2002). Over the continental margin, temperatures in the permanent halocline were about 2°C higher than normal in winter, and remained 1°C higher through summer 1998 (Smith et al., 2001; Huyer et al., 2002: see also Fig. 14a). The persistent La Niña of 1998-2000 is associated with negative steric height anomalies along the entire NH line that lingered for almost three years. But the weak El Niño of 2002-2003 was not associated with an increase in steric height off Newport. On the contrary, negative anomalies of steric height continued and even intensified in 2002, in spite of positive MEI values (Fig. 13). Even in 2003, most of the steric height anomalies over the continental margin remained negative, in spite of continuing weak El Niño conditions in the Equatorial Pacific. MEI values remained positive until the middle of 2005.

The negative steric anomalies in 2002 were associated with an unusually strong invasion of cool water from the northeastern Subarctic Pacific Ocean (Huyer, 2003). This event began with anomalous southward Ekman transport of Subarctic water into the North Pacific Current during January-February 2002 (Murphree et al., 2003). The eastward transport of the North Pacific Current was enhanced in late winter (Strub and James, 2003). There was also anomalously strong upwelling along the west coast of North America in spring and summer (Murphree et al., 2003), leading to a stronger California Current that was detected in satellite altimeter data (Strub and James, 2003). Along the central Oregon coast, the coastal upwelling jet forms the main core of the California Current (Lynn et al., 2003). Local observations by satellite-tracked drifters (Barth, 2003) and a mid-shelf mooring off Newport (Kosro, 2003) confirmed that the coastal jet was stronger than normal. This enhanced southward advection led to cooler, fresher waters in and above the halocline in the core of the California Current all along the west coast. These were detected in the summer of 2002 off southern California (Bograd and Lynn, 2003b) as well as on the NH line and Line P (Freeland et al., 2003). Since Subarctic waters are relatively high in nutrients, the enhanced southward advection resulted in higher than normal concentrations of chlorophyll (Wheeler et al., 2003; Thomas et al., 2003; Bograd and Lynn, 2003b).

Halocline temperature anomalies (Fig. 14a) provide a qualitative indication of the interrannual variability in the proportion of Subarctic water that is present on the NH line. We use the surface where salinity is 33.0 psu to represent the upper halocline; its depth ranges from the surface to 150 m (Fig. 14b). Anomalies were determined by subtracting the TENOC and LTOP seasonal cycles (Fig. 7) from the observed or vertically interpolated temperature on this isohaline. Negative anomalies indicate a higher percentage of Subarctic water, and positive anomalies indicate a lower percentage. Positive anomalies were prevalent at the beginning during the first few TENOC years, 1961-1964. Negative anomalies began during the La Niña of 1964-65 and were prevalent until 1967 (interrupted only by a weak positive event that began inshore in early 1966). Anomalies were near zero between 1967 and 1970, becoming negative again during the La Niña of 1970-71. Strong halocline temperature anomalies occurred during LTOP: positive anomalies >2°C occurred over the continental margin during the 1997-98 El

Niño, and negative anomalies of the same magnitude occurred during the Subarctic invasion of 2002. Negative anomalies persisted through September 2003, although this was an El Niño year with positive MEI values.

Time series of interannual anomalies in water mass properties are also available for Line P (1968-2004; Crawford et al, 2005) and for the CalCOFI region (1950-2000; Bograd and Lynn, 2003a). Summer temperature anomalies at 100-150 m depth on Line P show cool anomalies prevailing during 1968-1978, 1989-1992 and 2001-2004 (Crawford et al., 2005; their Fig. 9). Along CalCOFI Line 80 off Pt. Conception, properties of the 25.8 kg m^{-3} isopycnal surface indicate prevailing warm/salty anomalies during 1958-1964, 1979-1984, and 1997-2000, and prevailing cool/fresh anomalies during 1950-1958, 1967-1978, 1990-1995 (Bograd and Lynn, 2003a; their Fig. 10). Thus three regions of the California Current tend to show water mass anomalies of the same sign during the same or similar periods.

.

5. Seasonal and Interannual Variability of Nutrients, Chlorophyll and Copepods

Although nutrients were measured during TENOC, the sampling was limited; only four years (1966-1969) have regular seasonal sampling of nitrate. Summer and winter average sections were presented by Landry et al. (1989), and are not repeated here. Nitrate, phosphate and silicate were measured during the LTOP cruises and showed similar spatial and temporal patterns, so only the nitrate data is presented here (Fig. 15). Highest concentrations in the surface water occur inshore during the summer and fall. The offshore time series shows alternating bands of < 0.5 mmol m^{-3} nitrate (summer) and 2.0– 5.0 mmol m^{-3} nitrate (winter). A similar offshore pattern was recognized by Landry et al. (1989), but the higher resolution of the LTOP nitrate data allows a quantitative comparison of the seasonal variations in offshore surface nitrate concentrations. Nitrate concentrations in the upper halocline (33 psu) show significant interannual variation with two extremes: very low nitrate (10 mmol m^{-3}) in the warm, low salinity water during the 1997-1998 El Niño winter and very high (25 mmol m^{-3}) nitrate concentrations associated with the 2002 intrusion of Subarctic water (Wheeler et al. 2003). Inshore nitrate at 33 psu is high (20-25 mmol m^{-3}) during summer from equatorward flowing Subarctic water, but lower (10 mmol m^{-3}) during winter presumably due to the poleward flowing currents.

The LTOP time series for surface chlorophyll (chl) levels (Fig. 16a) shows the same general pattern seen in the nitrate distributions: maximum (2-20 mg chl m^{-3}) levels inshore during the summer, 0.5-1.0 mg chl m^{-3} offshore during the winter, and lowest (<0.5 mg chl m^{-3}) offshore during the summer. Chlorophyll estimates were also derived from SeaWiFS satellite data with 4x4 km horizontal resolution and 8-day composites, using the OC4 algorithm (O'Reilly et al. 2000). The higher spatial and temporal resolution of the SeaWiFS chlorophyll data better reflect the duration and extent of the elevated chl during the summer upwelling season (Fig. 16b). There are also hints of an earlier but smaller spring bloom that was not always sampled by the LTOP cruises (Fig. 15). The winter SeaWiFS data are more difficult to interpret due to frequent cloud cover. The remotely sensed chl was used to create a seasonal composite for 1997-2004 (Fig. 17a). The seasonal composite provides clear evidence of a small spring bloom in phytoplankton with maximum chl levels of 5 mg m^{-3} occurring between days 50 and 100. The faint representation of these spring blooms in the SeaWiFS time series (Fig.15b) is due to the small magnitude and short duration of the blooms. The 50-100 day duration of the spring bloom in the seasonal composite (Fig. 17a) probably reflects variable timing of the bloom depending on the time of the spring transition and the seasonal increase in solar radiation rather than the actual duration of a typical spring bloom. The spring bloom is usually dominated by *Thalassiosira* spp., *Actinopytchus* sp., and *Asterionellopsis glacialis* (Wetz et al., 2004). The seasonal composite also displays an extended summer bloom of phytoplankton between days 150 and 300 with maximum chl levels of 10 mg m^{-3} between days 200 and 250 (Fig. 17a). *In situ* observations indicate that this summer bloom is usually dominated by large diatoms (*Chaetoceros* spp.) and occasionally by smaller ones, e.g. *Leptocylindrus minimus* (Wetz and Wheeler, 2004).

At least two mechanisms can be invoked to explain the observed offshore seasonal pattern in chl. The first corresponds to actual changes in phytoplankton biomass and the second to changes in phytoplankton pigment levels occurring in response to varying light intensity. As seen in Fig. 17a, offshore waters display three ranges of chl concentrations; intermediate levels (~0.5 mg m^{-3}) from days 0-150, lowest chl levels (~0.2 mg m^{-3}) occurring between days 150 and 200, and highest levels (~0.75 mg m^{-3}) from days 275-325 (Fig. 17a). This seasonal pattern is similar to that observed offshore

in the Chile-Peru upwelling system for the austral winter and summer (Yuras et al., 2004). The intermediate chl levels during winter are likely due to the availability of sufficient nutrients with light limitation of phytoplankton growth due to reduced winter light levels and a deeper mixed layer (Corwith and Wheeler, 2002; Wetz et al., 2004). The lowest offshore chl values during summer are likely due to nitrogen limitation of phytoplankton growth which is intensified in our study region by the presence of the nutrient-depleted, highly-stratified Columbia River plume (Figs. 3b and 15a; Hill and Wheeler, 2002). The high offshore chl values observed later in the year may be related to the progressive offshore movement of the core of the coastal jet and the upwelling front (see Fig. 5).

Although temporal distributions of chl offshore are consistent with light limitation during winter (days 0-150) and nutrient limitation during summer (days 150-200), these changes in chl may be independent of changes in phytoplankton standing stocks measured as carbon biomass. Phytoplankton photoadaptation in regions of the Central North Pacific gyre during the winter lead to a two-fold increase in chl without an apparent change in phytoplankton carbon biomass (Letelier et al., 1993; Winn et al., 1995). Likewise, nitrogen limitation can also lead to a two-fold increase in the C:chl ratio of some flagellates (Herzig and Falkowski, 1989). Thus, seasonal variations of chl in offshore waters observed during LTOP may reflect changes in phytoplankton cell composition rather than actual changes in phytoplankton biomass.

The seasonal cycle of copepod biomass (Fig. 17, closed circles and line) and species richness calculated as the number of taxa observed in a given sample (Fig. 17, bars $\pm$ SE) are shown for the inner shelf station, NH-5 (from Hooff and Peterson, 2006). This copepod climatology is based on data from 1996-2004. Peak copepod biomass occurs in August and coincides with the maximum chl levels during the summer upwelling season. During summer, low species richness (~8) is associated with high biomass (20 mg C m^{-3}); during winter, species richness displays a maximum (~14) associated with low biomass (~5 mg C m^{-3}). The summer copepod community is dominated by cold-water neritic species that are representative of waters from the Bering Sea and coastal Gulf of Alaska. These include *Calanus marshallae, Pseudocalanus mimus, Acartia longiremis,* and *Centropages abdominalis* (Peterson and Miller, 1977).

Clearly the nutrient, chlorophyll, and copepod distributions show a strong seasonal pattern with maximum levels observed inshore during the summer. In the following section we will address the extent to which these patterns are directly linked to local or remote physical forcing factors and climate changes.

6. Biological Responses to Local and Remote Physical Forcing

Various ocean parameters of likely relevance to biological processes are compared in Figure 18 (for LTOP) and Figure 19 (for TENOC). These include time series of coho salmon survival (repeated from Figure 2), and time series of subsurface water properties at a station just offshore of the shelf-break (NH-25). For LTOP, we show time series of the vertically integrated chlorophyll averaged over the LTOP survey region which extends south from the NH line to 41.9°N, and from the coast to 126°W; spatial averaging of chlorophyll is appropriate because there are strong mesoscale gradients in surface properties (Huyer et al., 2005; Barth et al., 2005). No time series of chlorophyll are available for TENOC. Also included in Figures 18 and 19 are time series of proxies of the strength and direction of the alongshore coastal flow: for LTOP we used the difference between currents measured at 10 and 64 m by an acoustic Doppler profiler moored at NH-10 (Kosro, 2002; see also Appendix of Huyer et al., 2005); for TENOC we used geostrophic shear (0 to 30 m depth at NH-10) calculated from hydrographic data at NH-5 and NH-15. We also show time series of monthly mean values of local and large-scale climate indices: coastal upwelling anomalies (a measure of local wind forcing), coastal sea level at Crescent City (adjusted for the inverted barometer effect), shore temperature at Amphritite Pt.at 48.5°N on the coast of Vancouver Island, the Pacific Decadal Oscillation (PDO) and the multivariate ENSO index (MEI). During LTOP (Fig. 18), the time series of MEI, PDO, sea level anomaly and shore temperature anomaly are remarkably similar: all are positive during El Niño of 1997-8, negative during La Niña of 1998-2000, and positive during or soon after the weak El Niño of 2002-2003. During TENOC (Fig. 19), the similarities are less obvious: sea level and shore temperature anomalies seem to be associated with MEI but not with PDO. Using 40-year time series (1960-1999) Smith *et al*. (2000; their Table 3) found sea level anomalies to be associated with MEI but not PDO, though PDO and MEI are correlated with each other. Coastal

upwelling anomalies have much shorter time scales, with changes in sign occurring every few months.

It is clear from the time series of halocline temperature at NH-25 that the seasonal cycle dominates with cooler temperatures during the summer upwelling season and warmer temperatures during winter (Fig. 18; see also Fig. 7). The mean nitrate concentration in the halocline is 15 mmol m^{-3} with higher values in summer and lower values in winter. Our long-term observations indicate that the lowest nitrate values were during the 1997-98 El Niño (Corwith and Wheeler, 2002) and the highest nitrate values were recorded during the 2002 Subarctic intrusion (Wheeler et al., 2003). Phosphate follows a similar pattern (Fig. 18). For the LTOP time series the highest chl standing stocks appear to be related to increased levels of nitrate, phosphate and silicate in the halocline water (Wheeler et al., 2003). Similarly, low chl standing stocks are correlated with strong El Niño conditions (Corwith and Wheeler, 2002).

The halocline lies at a depth of about 100 m offshore and outcrops at the surface over the shelf in summer (Fig. 7). During summer upwelling, the onshore return flow over the shelf occurs in the middle of the water column rather than along the bottom (Huyer, 1983); this location coincides with the upper halocline. Thus the water of the upper halocline is an important source of surface-layer nutrients in summer. The temperature of the halocline shows seasonal oscillations (Fig. 18) related to the poleward flow during the winter and equatorward flow during the summer. Nitrate and phosphate are both elevated in the cooler halocline waters compared with the warmer halocline water (Fig. 18). During the 1997-98 El Niño winter, enhanced poleward flow of coastal water resulted in low nutrient concentrations and a lower N:P ratio than usually observed (Corwith and Wheeler, 2002). Thus the 1997-98 El Niño had two effects on nutrient supply: 1) enhanced downwelling and reduced upwelling off the Oregon coast (Fig. 18), and 2) enhanced poleward movement of warm, high salinity water with an anomalously low N:P ratio in the halocline (Corwith and Wheeler, 2002). In contrast, the enhanced Subarctic influence in 2002 resulted in cooler halocline temperatures and higher halocline nutrients all along the Oregon coast (Wheeler et al., 2003). This cold intrusion of Subarctic water apparently also diminished the local effects of the 2002-3 El Niño (Venrick et al., 2003).

Strong seasonal oscillations are apparent in the halocline temperature during TENOC (Fig. 19). Both nitrate and phosphate oscillate out of phase with the temperature variations, as seen during LTOP (Fig. 18). Although there are major gaps in the TENOC nutrient data set, we have sufficient nutrient data to compare halocline nutrient levels between the two time series. We grouped the data into "cool halocline" and "warm halocline" subsets to facilitate comparison of the equatorward flowing Subarctic waters and the poleward flowing warmer water (Table 2). The nitrate and phosphate concentrations and the N:P ratio were similar during both time series for the "warm halocline" water. Nitrate and phosphate concentrations in the "cool halocline" water were higher during LTOP than observed during TENOC, but the N:P ratios were similar (Table 2). These results indicate the variation in halocline nutrient concentrations are related to: 1) seasonal oscillations in alongshore currents (south during summer and north during winter) and 2) variations in the strength of the southward flowing current. During 1966-69 TENOC the sampling was frequent enough to clearly show nutrient concentrations increasing gradually within each upwelling season: the 4-year mean value of the seasonal increase in "cool halocline" nutrient level was 4.8 mmol m^{-3} for nitrate and 0.38 mmol m^{-3} for phosphate.

As noted by Huyer et al. (2003), the enhancement of the Subarctic flow in 2002 was more exteme than any prior observation. Nutrient levels and chl standing stocks remained elevated in 2003 (Fig. 18), so it is possible that the higher nutrient levels in the LTOP "cool halocline" are primarily a result of this recent Subarctic intrusion. Indeed, if the 2002-2003 data is excluded from the TENOC/LTOP comparisons, the difference in nutrient levels is no longer statistically significant (Table 2).

The observed seasonal cycle for chl and copepod standing stocks suggests a strong link between upwelling conditions, nutrient supply, primary production by phytoplankton and secondary production by zooplankton. However, there is no significant correlation between interannual variations in chlorophyll and the copepod standing stocks measured at NH-5. The highest copepod standing stocks between 1996 and 2005 were reported for 2000-2001 (Hooff and Peterson, 2006) while the highest chl concentrations were observed in 2002 (Fig. 16; Wheeler et al., 2003). There could be several explanations for an apparent lack of coupling between the phytoplankton

response to increased nutrients and a zooplankton response to an increased food supply. First, there are significant lags between the wind forcing and the ecosystem responses. Model simulations for the 2001 upwelling season (Spitz et al., 2005) indicate that the respective time lags are: wind stress and nitrate (3 days), wind stress and phytoplankton (7 days) and wind stress and zooplankton (13-16 days). Model results (Spitz et al., 2005) also examine variations in the spatial distribution of phytoplankton and zooplankton depending on the particular upwelling/downwelling conditions within the upwelling season. During upwelling high mean values of chlorophyll are in the surface layer inshore of the 50 m isobath. Over the same time period relatively high mean zooplankton standing stocks are in the surface layer offshore of the jet and offshore of the local maximum in mean chl. This spatial distribution is altered during a weak downwelling event when the largest mean zooplankton standing stocks are found close to shore and inshore of the jet. During upwelling, phytoplankton stocks increase inshore while zooplankton increase further offshore. During downwelling, grazing by zooplankton is larger than accumulation of phytoplankton from physical forcing, and thus phytoplankton decrease along the coast. Although nutrients, phytoplankton and copepods were sampled simultaneously during the LTOP cruises, the differences in lag times for biological responses could obscure correlations between the two responses.

A second factor that could explain the uncoupling between phytoplankton abundance and copepod standing stocks is differences in life cycle and seasonal reproduction. The cold-water neritic copepods are constrained by a seasonal life history and may not be able to establish high standing stocks unless reproduction is started by early spring. Although total copepod biomass was low in 2002, the anomaly in cold-water copepod species increased from 1999-2002 and reached a maximum in 2002 (Mackas et al., 2006). In contrast, the southern warm-water copepods are more opportunistic and once established may produce multiple generations if food is available. El Niño conditions are characterized by low chlorophyll, low copepod biomass, and high warm-water species anomalies without the lag in response observed for the northern species (Mackas et al. 2006).

A third factor that could explain the apparent uncoupling between physics and the response of distinct trophic levels is the biological control of the ecosystem structure.

Most of our present analyses and interpretations do not take into account the interactions among distinct heterotrophic components. These interactions may be particularly important when interpreting time series with sampling intervals longer than the generation time of dominant assemblages.

7. Conclusions

Unlike its northern and southern sisters (Line P and CalCOFI), the Newport Line is largely in the coastal domain, and thus especially subject to strong seasonal forcing by local winds and to remote forcing from the Equatorial Pacific through the coastal wave guide. And unlike its sister programs, the NH Line sampling was designed at the outset, mid-1961, to resolve spatial variation in the coastal ocean, with station spacing of 10 nm over the continental margin and 20 nm offshore. Seasonal sampling with bimonthly or more frequent sections continued for about ten years. Specific questions arose while the sampling continued and technology developed. By the end of 1971 routine monitoring was replaced by a long series of process studies to investigate issues which had been only dimly understood. Many of these explored the physical dynamics of wind-forced circulation over and along the continental margin. By the time routine seasonal sampling of the NH-line resumed under the auspices of the GLOBEC Northeast Pacific program, these process studies had already provided a basic understanding (e.g., Huyer, 1990; Hickey, 1998) of many physical phenomena: coastal upwelling including the upwelling front and baroclinic coastal jet; winter downwelling and the associated northward current; the seasonal variation of coastal currents including the rapid spring and fall transitions; the Columbia River plume which is advected southwestward across the NH line in summer; and coastal trapped waves in carrying signals from farther south (including equatorial perturbations such as El Niño and La Niña) to Oregon coastal waters. Each of these phenomena affects conditions in the coastal ocean off Newport, regularly or intermittently, and all have proven to be important in interpreting our TENOC and LTOP time series. Recent process studies (e.g., Barth and Wheeler, 2005) have addressed more sophisticated or difficult questions, such as the role of alongshore variations in topography, the importance of spatial variations in the wind stress, and biophysical

interactions. These too have guided our interpretation, but much remains to be learned, particularly about the biological interactions in the coastal ocean.

Seasonal variations dominate the physical characteristics (temperature, salinity, density, and velocity) down to depths of at least 150 m during both TENOC and LTOP. Nutrient concentrations also vary seasonally, particularly in the surface layer. In the halocline, higher nutrient concentrations and higher nitrate-to-phosphate ratios are associated with lower temperatures and southward surface currents, i.e., with higher concentrations of Subarctic water carried southward seasonally by the coastal upwelling jet. Conversely, lower nutrient concentrations and lower nitrate-to-phosphate ratios in the halocline are associated with higher temperatures and northward currents. The seasonal variation of nutrients is associated with seasonal changes in the phytoplankton biomass estimated from the LTOP surveys and the SeaWiFS satellite. Both the seasonal chlorophyll cycle and the seasonal cycle in alongshore currents seem important to the copepod biomass (which peaks in summer when nutrients are plentiful) and diversity which peaks in winter (when warmer waters and subtropical species are advected northward).

The TENOC and LTOP data sets were sufficiently compatible in their spatial and temporal sampling to enable us to make a statistical comparison of physical conditions along the NH line in two epochs whose mid-points are separated by 35 years. Except at the most offshore station sampled by both programs (NH-85), the very strong seasonal variability precludes estimating long-term change by pooling data from all seasons. Comparison of TENOC and LTOP summers shows: significant warming in the seasonal thermocline and in a subsurface region just offshore of the shelf-break; significant freshening along the sloping halocline over the continental margin; and a significant rise in steric height (surface elevation) over the continental slope. Comparison of TENOC and LTOP winters also shows warming of the surface layer and freshening of the halocline, but differences are not statistically significant because of high interannual variability during LTOP. The pooled data from NH-85 also shows significant warming at most depths shallower than 500 m. Warming of the upper ocean has also been observed on both Line P and CalCOFI Lines 80 and 90 – thus we see that the upper layer of the entire California Current system is appreciably warmer than it was 35 years ago. Given the very

large gap (1970-1997) in regular sampling of the NH line, our data set cannot adequately address the question of how this change occurred. Large-scale climate studies (Hare et al., 2000; Bond et al., 2003; Schwing et al., 2005) indicate that important "regime shifts" occurred in about 1977, 1989 and 1998. Between 1965 and 1989, the PDO pattern was clearly dominant; its sign switched in 1976 and 1989 (from negative to positive and back again (Hare et al., 2000; Bond et al., 2003). Since 1990, another pattern has beeen dominant: its sign switched from negative to positive in 1998 (Bond et al., 2003). These climate regime shifts seem to be reflected in the 50-year time series of oceanographic sampling along Line P and CalCOFI Lines 80 and 90 (Schwing *et al.*, 2005).

Interannual variability was considerably higher during LTOP than TENOC, particularly in winter. We found a significant increase in the winter temperature variance over the outer continental shelf and upper slope. Winter steric heights are also more variable during the recent epoch. A variance increase is seen in coastal upwelling indices and large-scale climate indices (MEI, PDO) as well as in the coastal ocean. No signals as strong as either the El Niño in the winter of 1997-98 nor the unusual Subarctic intrusion in 2002 occurred during the earlier epoch. On the contrary, seasonal variability was stronger and more regular during the earlier epoch. We do not know if this increase in interannual variability is a harbinger of extreme events to come. Many climate models suggest that the frequency and intensity of extreme events is likely to increase in association with the global warming anticipated over the coming decades (Easterling et al., 2000). Bakun (1990) has suggested that summer upwelling could intensify; perhaps the very high values of the 2001-2003 values of the coastal upwelling index at 42°N are evidence of this effect.

Water mass properties including nutrient concentrations of the upper ocean also exhibited more interannual variability during LTOP than TENOC. The halocline was particularly warm and nutrient-poor during winter and spring of 1998, following the peak of El Niño 1997-98. The halocline was particularly cool and nutrient-rich in the upwelling seasons of 2002 and 2003, during and after the major Subarctic invasion of 2002. These interannual variations in the nutrient concentrations of upwelling-source waters are reflected in the chlorophyll concentrations detected by the SeaWiFS satellite and in regional averages of the *in situ* measurements. We were not able to relate these

variations in nutrients and phytoplankton biomass to interannual variations in the available estimates of copepod biomass, perhaps because a long time-series is available only for one location (NH-5 over the inner shelf) which may not be representative of this coastal ecosystem, given the patchy nature of plankton populations. It is also possible that the longer time scales relevant for zooplankton growth would obscure any simple relationship, or that biological interactions among trophic levels are dominant.

Salmon survival improved during the LTOP period, from a low of <1% for smolts released in 1997, to about 4% for smolts released in 2000 and 2002, but survival rates remain much lower than they were during TENOC. It seems unlikely that the large reduction in salmon survival rates, from 6.1±2.1% during TENOC to 2.5±1.3% during LTOP, can be fully explained by the quite subtle long term changes in oceanographic conditions we observed along the Newport Line. A variety of anthropogenic activities could also have had negative effects on the riparian and marine habitats. Logging in both the Oregon Coast Range and the Cascade Range likely reduced water quality and increased water temperature in small streams. Damming of larger rivers and streams for flood control and irrigation has significantly changed the seasonal streamflow pattern of the Columbia River (Sherwood et al., 1990), increasing discharge during autumn and winter, and reducing the rate and quantity of discharge during the spring season when smolts are released. Streamflow regulation began in 1969 (near the end of TENOC) and was fully implemented by 1975 (well before LTOP). Whether and how streamflow regulation affects salmon survival remain controversial issues. Nevertheless, we cannot rule out the possibility that the marine environment is an important determinant of salmon survival.

Given the importance of the coastal ecosystem to marine life and to human communities, we hope and expect that monitoring of the coastal ocean off Oregon will continue. Future monitoring efforts in this region will need to be designed very carefully. Care must be taken to avoid aliasing by the strong seasonal cycle and by the strong wind-driven fluctuations over the continental shelf and slope. Some monitoring can be done remotely (e.g., by satellites, coastal radar, moorings, and autonomous vehicles such as gliders), but many more sophisticated questions will require shipboard measurements. Our analysis of the NH line data sets suggests that the shelf-break station NH-25 is an

excellent site to monitor the quality of upwelling source waters. It also suggests that monitoring for long-term climate change need not be continuous: it might be sufficient to have 5-10 year periods with intense seasonal monitoring separated by a decade of low-level monitoring. Ideally, the low-level monitoring should be sufficiently intense to detect the onset of extreme events, and include options for increased sampling at short notice . Experiments and process studies will be needed to evaluate the physiological status of phytoplankton in different seasons and in different environments, to determine the optimum duration and intensity of upwelling/downwelling cycles for maximum primary production, and to determine the relative importance of various zooplankton classes (e.g., copepods and euphasiids) to the overall secondary production that supports higher trophic levels. To address the important ecosystem questions, future monitoring and process studies will need to be even more interdisciplinary and more sophisticated than our GLOBEC LTOP time series. Our work here provides a solid foundation for future monitoring.

Acknowledgments

We are very grateful to the many people who participated in the TENOC and GLOBEC LTOP cruises. Jane Fleischbein, Jennifer Jarrell Wetz, Jasmine Nahorniak, Corinne James and Martin Saraceno all assisted us with data analysis. Jack Barth, Bill Peterson, Steve Pierce, Evelyn and Barry Sherr provided supplementary CTD data from process studies during the LTOP period. Bill Pearcy and Joe Fisher provided the salmon survival data. Upwelling and large-scale climate indices are generously provided to the community through the internet by Frank Schwing and colleagues at the Pacific Environmental Laboratory (CUI), by Nate Mantua at University of Washington (PDO), and Klaus Wolter at National Center for Atmospheric Research (MEI). We thank Bill Peterson and Dudley Chelton for helpful discussions, and three anomymous reviewers for valuable comments. We are supported by the National Science Foundation through Grant 0434810-OCE. This is a contribution of the U. S. GLOBEC program, jointly funded by the National Science Foundation and the National Oceanic and Atmospheric Administration.

Appendix: THE DATA

The comparable time-series data for the periods 1961-1971 (TENOC) and 1997-2005 (LTOP) are the physical oceanographic data from hydrographic casts (temperature and salinity vs. depth) made at stations along the Newport Line (Figure 1). During TENOC, hydrographic casts were made with bottles and reversing thermometers at standard depths (Smith et al., 2001). The temperature data from TENOC are estimated to be accurate to +/- 0.02 C. The salinity was determined using an inductive salinometer in the shore laboratory after 1962 and is estimated to be accurate to 0.003 ppt, but prior to 1962 salinity was determined by titration with estimated accuracy of 0.02 ppt. Although the international definition of salinity changed between TENOC and LTOP, quantitative differences between the old salinity scale (units of gm kg^{-1}, i.e., ppt) and the new Practical Salinity Scale 1978 ('practical salinity units' or psu) are very small (Lewis and Perkin, 1981); we have neglected these small differences. Sampling during LTOP was done with a dual-sensor CTD and rosette sampler and accuracies are better than 0.01C, 0.003 psu, and 1db. A comparison of mean temperature and salinity measured at the greatest common depth (1000 m) from the farthest seaward common station (NH-85) during TENOC and during LTOP gives confidence in the different measurement techniques: The mean and standard deviation of the temperature and salinity at 1000 m from 54 TENOC samples is T = 3.56 C +/- 0.11 C, S = 34.417 +/- 0.021, and from 37 LTOP samples is T = 3.62 C +/- 0.08 C and S = 34.407 +/- 0.015.

Since the steric height is computed as the depth (pressure) integral of specific volume (a function of temperature and salinity), it is conceivable that steric height estimated from discrete samples at fewer than 20 standard depths (as in TENOC) would differ from that estimated from nearly continuous profiles with depth (during LTOP). As a test, we re-computed the LTOP steric heights using only the CTD T, S data sub-sampled at standard depths. We compared the steric height from sub-sampled data with the steric heights computed using data at 1-meter (1 db) intervals for the 53 stations where steric height relative to 500 db could be computed without extrapolation. (The steric height ranged from 80.0 to 100.2 cm for the 53 pairs). The mean difference between the usual LTOP steric height and that computed from sub-sampled (13 standard depths) data was 0.33 cm (and rms difference of 0.48 cm), with individual differences

ranging between -0.40 and +1.30 cm, which is small compared to the temporal and spatial variability observed.

Property/property plots were compared for nitrate vs temperature and nitrate vs salinity at the shelf break station (NH-25) to determine if there were any significant differences in the nutrient concentrations between the TENOC and LTOPS data sets. The TENOC data set has a lower slope for the nitrate vs. temperature regression for temperatures $\leq 10\ ^{o}C$:

TENOC: $y = [89.8376 \pm 4.56388] + [-8.70266 \pm 0.52666]x.$

LTOP: $y = [113.969 \pm 8.25406] + [-11.081 \pm 0.93536]x.$

Both data sets have nearly identical nitrate vs. salinity regressions:

TENOC: $y = [-506.895 \pm 10.3522] + [15.7831 \pm 0.314692]x$

LTOP: $y = [-544.535 \pm 25.4739] + [16.9607 \pm 0.776707]x$

We also compared phosphate vs. temperature and phosphate vs. salinity at NH-25. The TENOC data set has a lower slope for the phosphate vs. temperature regression for temperatures $\leq 10\ ^{o}C$:

TENOC: $y = [5.91335 \pm 0.233576] + [-0.528067 \pm 0.022948]x.$

LTOP: $y = [7.78182 \pm 0.394525] + [-0.714222 \pm 0.0447431]x.$

The TENOC data set also has a lower slope for the phosphate vs. salinity regression:

TENOC: $y = [-22.5946 \pm 0.692595] + [0.724856 \pm 0.0211039]x.$

LTOP: $y = [-34.2006 \pm 1.21125] + [1.0794 \pm 0.0369056]x.$

References

Allen, J.S. (1980). Models of wind-driven currents on the continental shelf. *Ann. Rev. Fluid Mech., 12*, 389-433.

Anderson, I., Huyer, A., Smith, R.L. (1983). Near-inertial motions off the Oregon coast. *J. Geophys. Res., 88*, 5960-5972.

Austin, J.A., Barth, J. A. (2002). Variation in the position of the upwelling front on the Oregon shelf, *J. Geophys. Res., 107*, 3180, doi:10.1029/2001JC000858.

Bakun, A. (1973). Coastal upwelling indices, West Coast of North America, 1946j-71. U.

S. Dept of Commerce, National Oceanic and Atmospheric Administration. NOAA Tech. Rep. NMFS SSRF-671, Seattle, 114 pp.

Bakun, A. (1990). Global climate change and intensification of coastal ocean upwelling. *Science, 247,* 198-201.

Barnes, C. A., Duxbury, A.C., Morse, B.-A. (1972). Circulation and selected properties of the Columbia River effluent at sea. In: *The Columbia River Estuary and Adjacent Ocean Waters, Bioenvironmental Studies,* edited by A.T. Pruter and D. L. Alverson, University of Washington Press, Seattle, 41-80.

Barth, J.A. (2003). Anomalous southward advection during 2002 in the northern California Current: Evidence from Lagrangian Surface drifters. *Geophysical Research Letters, 30,* 8024, doi:10.1029/2003GL017511.

Barth, J. A., Pierce, S.D., Cowles, T.J. (2005). Mesoscale structure and its seasonal evolution in the northern California Current system. *Deep-Sea Research II, 52,* 5-28.

Barth, J.A., and Wheeler, P.A. (2005). Introduction to special section: Coastal Advance in Shelf Transport. *J. Geophys. Res., 110,* C10S01, doi:10.1029/2005JC003124.

Bograd, S.J., Lynn, R.J. (2003a). Long-term variability in the southern California Current system. *Deep Sea Research II, 50,* 2355-2370.

Bograd, S.J., Lynn, R.J. (2003b). Anomalous Subarctic influence in the southern California Current during 2002. *Geophysical Research Letters,* 30, 8020, doi:10.1029/2003GL17446.

Bond, N. A., Overland, J.E., Spillane, M., Stabeno, P. (2003). Recent shifts in the state of the North Pacific. *Geophysical Research Letters, 30,* 2183, doi:10.1029/2003GL018597.

Burt, L., Ludwig, M. (1998). Oceanography at Oregon State University: The First Two Decades: 1954-1975. Oregon State University, Corvallis. 225 pp.

Castelao, R.M., Barth, J.A. (2005). Coastal ocean response to summer upwelling favorable winds in a region of alongshore bottom topography variations off Oregon. *J. Geophys. Res., 110,* 10S04, doi: 10.1029/2004JC002409.

Chelton, D.B., Schlax, M.G. (1996). Gobal observations of oceanic Rossby waves. *Science, 202,* 234-238.

Corwith, H.L., Wheeler, P.A. (2002). El Niño related variations in nutrient and chlorophyll distributions off Oregon. *Progress in Oceanography, 54,* 361-380.

Crawford, W., Sutherland, P., van Hardenberg, P. (2005). Cold water intrusion in the eastern Gulf of Alaska in 2002. *Atmosphere-Ocean*. *43***,** 119-128.

Curtin, T.B., Mooers, C.N.K. (1975). Observation and interpretation of a high-frequency internal wave packet and surface slick pattern, *J. Geophys. Res.*, *80*, 882-894.

Denbo, D.W., Allen, J.S. (1987). Large-scale response to atmospheric forcing of shelf currents and coastal sea level off the west coast of North America: May-July 1981 and 1982, *J. Geophys. Res.*, *92*, 1757-1782.

Easterling, D.R., Meehl, G.A., Parmesan, Changnon, C.S.A., Karl, T.R. Mearns, L.O. (2000). Climate extremes: Observations, modeling, and impacts. *Science, 289*, 2068-2074.

Emlen, J.M., Reisenbichler, R.R., McGie, A.M., Nickelson, T.E. (1990). Density-dependence at sea for Coho salmon (*Oncorhyncus kisutch*). *Can. J. Fish. Aquat. Sci., 47*, 1765-1772.

Erofeeva, S.Y., Egbert, G.D., Kosro, P.M. (2003). Tidal currents on the central Oregon shelf: Models, data, and assimilation, *Journal of Geophysical Research*, *108*, 3148, doi:10.1029/2002JC001615.

Francis, R. C., Hare, S.R. (1994). Decadal-scale regime shifts in the large marine ecosystems of the North-east Pacific: a case for historical science. *Fisheries Oceanography*, *3*, 279-291.

Freeland, H.J., Gatien, G., Huyer, A., Smith, R.L. (2003). Cold halocline in the northern California Current: An invasion of Subarctic water. *Geophysical Research Letters, 30*, 1141, doi:10.1029/2002GL016663.

Fu, L.-L. (2004). Latitudinal and frequency characterists of the westward propagation of large-scale oceanic variability. *J. Phys. Oceanogr., 34*, 1907-1921.

Gan, J., Allen, J.S. (2005). Modeling upwelling circulation off the Oregon coast, *J. Geophys. Res., 110*, C10S07, doi:10.1029/2004JC002692.

Halpern, D. (1976). Structure of a coastal upwelling event observed off Oregon during July 1973, *Deep-Sea Res., 23*, 495-508.

Hare, S.R., Mantua, N.J. 2000. Empirical evidence for North Pacific regime shifts in 1977 and 1989. *Progress in Oceanography*, *47*, 103-145.

Herzig, R., Falkowski, P.G. 1989. Nitrogen limitation in *Isochrysis galbana* (Haptophyceae) I. Photosynhtetic energy conversion and growth efficiencies. *J. Phycol., 25, 462-471.*

Hickey, B.M. (1998). Coastal oceanography of western North America from the tip of Baja California to Vancouver Island, in *The Sea. The Global Coastal Ocean: Regional Studies and Syntheses*, edited by A. R. Robinson and K. H. Brink, pp. 345-393, John Wiley & Sons, Inc, New York.

Hill, J. K., Wheeler, P.A. (2002). Organic carbon and nitrogen in the northern California Current system during July 1997: comparison of offshore, river plume, and coastally upwelled water. *Progress in Oceanography*, 53, 369-387.

Hooff, R. C., Peterson, W.T. (2006). Copepod biodiversity as an indicator of changes in ocean and climate conditions of the northern California Current ecosystem. Limnol. Oceanogr., *in press*.

Huyer, A. (1976). A comparison of upwelling events in two locations: Oregon and Northwest Africa. *J. Marine Res.*, 34: 531-546.

Huyer, A. (1977). Seasonal variation in temperature, salinity and density continental shelf off Oregon. *Limnol. Oceanogr., 22*, 442-453.

Huyer, A. (1983). Coastal Upwelling in the California current system. *Progress in Oceanography, 12*, 259-284.

Huyer, A. (1990). Shelf circulation. In: *The Sea, Vol 9: Ocean Engineering Science,* pp. 423-466, edited by B. Le Mehaute and D. M. Hanes. Wiley.

Huyer, A. (2003). Preface to special section on enhanced Subarctic influence in the California Current, 2002. *Geophysical Research Letters, 30*, 8019, doi:10.1029/2003GL017724.

Huyer, A., Fleischbein, J.H., Keister, J., Kosro, P.M., Perlin, N., Smith, R.L., Wheeler, P.A. (2005). Two coastal upwelling domains in the northern California Current system. *Journal of Marine Research, 63*, 901-929.

Huyer, A., Smith, R.L. (1974). A subsurface ribbon of cool water over the continental shelf off Oregon. J. Phys. Oceanogr., 4(3):381-391.

Huyer, A., Smith, R.L. (1985). The signature of El Niño off Oregon, 1982-83. *J. Geophys. Res., 90*, 7133-7142.

Huyer, A., Smith, R.L., Fleischbein, J. (2002). The coastal ocean off Oregon and Northern California during 1997-8 El Niño. *Progr. Oceanogr., 54*, 311-341.

Huyer, A., Sobey, E.J.C., Smith, R.L. (1979). The spring transition in currents over the Oregon continental shelf. *J. Geophys. Res., 84*, 6995-7011.

Klymak, J.M., Moum, J.M. (2003). Internal solitary waves of elevation advancing on a

shoaling shelf, *Geophysical Research Letters, 30*, 2045, doi:10.1029/2003GL017706.

Koslow, J.A, Hobday, A.J., Boehlert, G.W. (2002). Climate variability and marine survival of coho salmon (Oncorhynchus kisutch) in the Oregon production area *Fisheries Oceanography*, *11***,** 65-77**.**

Kosro, P.M. (2002). A poleward jet and an equatorward undercurrent observed off Oregon and northern California during the 1997-98 El Niño, Progr. Oceanogr., *54*, 343-360.

Kosro, P.M. (2003). Enhanced southward flow over the Oregon shelf in 2002: a conduit for subarctic water. *Geophysical Research Letters, 30*, 8023, doi:10.1029/2003GL017436.

Kosro, P.M. (2005). On the spatial structure of coastal circulation off Newport, Oregon during spring and summer 2001 in a region of varying shelf width. J. Geophys. Res., *110*, C10S06, doi:10.1029/2004JC002769.

Kurapov, A.L., Egbert, G.D., Allen, J.S., Miller, R.N,, Erofeeva, S.Y., Kosro, P.M. (2003). The M2 Internal Tide off Oregon: Inferences from data assimilation, *Journal of Physical Oceanography, 33*, 1733-1757.

Kurapov, A.L., Allen, J.S., Egbert, G.D,, Miller, R.N, (2005). Modeling bottom mixed layer variability on the mid-Oregon shelf during summer upwelling, *Journal of Physical Oceanography*, *35*, 1629-1649.

Landry, M.R., J.R. Postel, W.K. Peterson and J. Newman. 1989. Broad-scale distributional patterns of hydrographic variables on the Washington/Oregon shelf. In: Coastal Oceanography of Washington and Oregon, edited by M. R. Landry and B. M. Hickey, Elsevier, Amsterdam, pp. 1-40.

Letelier, R.M., Bidigare, R.R., Hebel, D.V., Ondrusek, M., Winn, C.D., Karl, D.M. (1993). Temporal variability of the phytoplankton community structure based on pigment analyses. *Limnol. Oceanogr., 38*, 1420-1437.

Lewis, E.L., Perkin, R.G. (1981). The Practical Salinity Scale 1978: conversion of existing data. Deep-Sea Research, 28, 307_328.

Lynn, R.J., Bograd, S.J., Chereskin, T., Huyer, A. (2003). Seasonal renewal of the California Current: the spring transition off California. *J. Geophys. Res., 108*, 3279, doi:10.1029/2003JC001787.

Mackas, D.L., Peterson, W.T., Ohman, M.D., Lavaniegos, B.E.. (2006). Zooplankton anomalies in the California Current system before and during the warm ocean conditions of 2005. *Geophys. Res. Lett*. Submitted .

Mantua, N.J., Hare, S.R., Zhang, Y., Wallace, J.M., Francis, R.C. (1997). A Pacific interdecadal climate oscillation with impacts on salmon production. *Bull. Amer. Meteor. Soc., 78*, 1069-1079.

McGowan, J.A., Cayan, D.R., Dorman, L.M. (1998). Climate-ocean variability and ecosystem response in the Northeast Pacific. *Science*, *281*, 210-217.

Miller, A.J., Cayan, D.R., Barnett, T.P., Graham, N.E., Oberhuber, J. M. (1994). The 1976-77 climate shift of the Pacific Ocean. *Oceanography, 7*, 21-26.

Mooers, C.N.K, Collins, C.A., Smith, R.L. (1976). The dynamic structure of the frontal zone in the coastal upwelling region off Oregon, *J. Phys. Oceanogr., 6*, 3-21.

Murphree, T., Bograd, S.J., Schwing, F.B., Ford, B. (2003). Large-scale atmosphere-ocean anomalies in the Northeast Pacific during 2002. *Geophysical Research Letters, 30*, 8026, doi:10.1029/2003GL017303.

Nelson, C.S., Husby, D.M. (1983). Climatology of surface heat fluxes over the California Current region. U.S. Dept. of Commerce., NOAA Tech. Rep. NMFS SSRF-763. 155 pp.

O'Reilly, J.E., and others. (2000). Ocean color chlorophyll a algorithms for SeaWiFS OC2 and OC4, Version 4. In S.B. Hooker and E. R. Firestone [eds.], SeaWiFS postlaunch calibration and validation analysis. Part 3. NASA Technical Memo 2000-206892, V. 11, NASA Goddard Flight Center.

Pak, H., Beardsley, G.F. Jr., Park, P.K. (1970). The Columbia River as a source of marine light scattering particles. *J. Geophys. Res., 75*, 4570-4578.

Peterson, W.T., Miller, C.B. (1977). Seasonal cycle of zooplankton abundance and species composition along the central Oregon coast. *Fish. Bull. U. S., 75*, 717-724.

Pierce, S.D., Smith, R.L., Kosro, P.M., Barth, J.A., Wilson, C. D. (2000). Continuity of the poleward undercurrent along the eastern boundary of the mid-latitude north Pacific. *Deep-Sea Res. Part II, 47*, 811-829.

Reid, J.L. (1965). Intermediate waters of the Pacific Ocean. *The Johns Hopkins Oceanographic Studies, 2*, 85 p.

Reid, J.L., Mantyla, A.W. (1976). The effect of geostrophic flow upon coastal sea elevations in the northern North Pacific Ocean. *J. Geophys. Res., 81*, 3100-3110.

Schwing, F., Batchelder, H., Crawford, W., Mantua, N., Overland, J., Polovina, J., Zhao, J.-P. (2005). Decadal-scale climate events. (2005). In: Report of the Study Group

on Fisheries and Ecosystem Responses to Recent Regime Shifts, edited by J. R. King, PICES Scientific Report No. 28. North Pacific Marine Science Organization, Sidney, B. C. pp. 1-36.

Sherwood, C. R., Jay, D., Harvey, R.B., Hamilton, P., Simenstad. C.A. (1990). Historical changes in the Columbia River estuary. *Prog. Oceanogr., 25,* 299-352.

Smith, R.L., Huyer, A., Fleischbein, J. (2001). The coastal ocean off Oregon from 1961 to 2000: Is there evidence of climate change or only of Los Niños? *Progress in Oceanography, 49*, 63-93.

Snedecor, G.W., Cochran, W.G. (1967). *Statistical Methods, 6th edition*. Iowa State University Press, Ames, Iowa. 593 pp.

Spitz, Y.H., Allen, J.S., Gan, J. (2005). Modeling of ecosystem processes on the Oregon shelf during 2001 upwelling. *J. Geophys. Res., 110*, C10S17, doi:10.1029/2005JC002870.

Strub, P.T., James, C. (2002). Altimeter-derived surface circulation in the large-scale NE Pacific Gyres. Part 1. Seasonal variability. *Progress in Oceanography, 53*, 163-183.

Strub, P.T., James, C. (2003). Altimeter estimates of anomalous transports into the northern California Current duing 2000-2002. *Geophyical Research Letters, 30*, 8025, doi:10.1029/2003GL017513.

Tabata, S., Thomas, B., Ramsden, D. (1986). Annual and interannual variability of steric sea level along Line P in the Northeast Pacific Ocean. *J. Phys. Oceanogr.*, ***16***, 1378-1398.

Talley, L.D. (1993). Distribution and formation of North Pacific Intermediate Water. *J. Phys. Oceanogr., 23*, 517-537.

Taylor, G.H., Hannan, D. (1999). *The Climate of Oregon.* Oregon State University Press, Corvallis, Oregon. 211 pp.

Thomas, A.C., Strub, P.T., Brickley, P. (2003). Anomalous satellite-measured chlorophyll concentrations in the northern California Current in 2001-2002. *Geophysical Research Letters, 30*, 8022, doi:10.1029/2003GL017409.

Torgrimson, G. M., Hickey, B. M. (1979). Barotropic and baroclinic tides over the continental slope and shelf off Oregon, *J. Phys. Oceanogr., 9*, 945-961.

Venrick, E., et al. (2003). The state of the California Current, 2002-2003: Tropical and Subarctic influences vie for dominance. *CalCOFI Rep., **44***, 28-60.

Wetz, M. S., Wheeler, P. A. (2004). Response of bacteria to simulated upwelling phytoplankton blooms. *Marine Ecology Progress Series, 272,* 49-57.

Wetz, M. S., Wheeler, P.A., Letelier, R.M. (2004). Light-induced growth of phytoplankton collected during the winter from the benthic boundary layer off Oregon. *Mar. Ecol. Prog. Ser., 280,* 95-104.

Wheeler, P. A., Huyer, A., Fleischbein, J. (2003). Cold halocline, increased nutrients and higher chlorophyll off Oregon in 2002. *Geophys. Res. Lett., 30,* 8021, doi: 10.1029/2003GL017395.

Whitney, F., Freeland, H.J. (1990). Variability in upper ocean water properties in the NE Pacific Ocean. *Deep-Sea Res. Part II, 46,* 2351-2370.

Winn, C. D., Campbell, L., Christian, J., Letelier, R.M., Hebel, D.V., Dore, J. E., Fujieki, L., Karl, D.M. (1995). Seasonal variability in the phytoplankton community of the North Pacific subtropical gyre. *Global Biogeochemical Cycles, 9,* 605-620.

Wolter, K., Timlin, M.S. (1998). Measuring the strength of ENSO – how does 1997-8 rank? *Weather, 53,* 315-324.

Yuras, G., Ulloa, O., Letelier, R., Pizarro, O. (2004). On the annual cycle of chlorophyll off Chile (18°-40°S). Gayana (Concepc.) v.68 n.2 supl. TIIProc. Conception, p.611-614. ISSN 0717-6538.

Table 1. Comparison of seasonal values of selected climate indices during TENOC and LTOP. Coastal wind stress is represented by the coastal upwelling indices (CUI) at 45 N, 125 W, and at 42 N, 125 W. Monthly values of the CUI are provided by Pacific Fisheries Environmental Lab. ; units are cubic meters per 100 m of coast-line. The multivariate ENSO Index (MEI) represents conditions in the Equatorial Pacific Ocean (Wolter and Timlin (1998); bi-monthly values are provided by Klaus Wolter, The Pacific Decadal Oscillation represents conditions in the Pacific Ocean north of 20°N (Mantua et al., 1997); monthly values are provided by Nate Mantua. For each variable, monthly values were combined to give seasonal estimates for summer (July and August) and winter (January and February

		Average ± SE			Variance		
		1961-71	1997-2005	Diff.	61-71	97-05	Ratio
Jul-Aug CUI	45 N	65.91 ± 7.16	68.89 ± 7.33	2.98	563	483	0.86
	42 N	128.27 ± 13.98	193.11 ± 22.93	64.84	2149	4733	2.20
Apr – Jun CUI	45 N	38.33 ± 6.34	21.59 ± 4.05	-16.74	446	147	0.33
	42 N	94.09 ± 11.47	97.11 ± 13.75	3.02	1447	1701	1.18
July-Aug MEI		-0.25 ± 0.27	0.47 ± 0.17	0.72	0.78	0.26	0.33
July- Aug PDO		-0.68 ± 0.16	0.20 ± 0.38	0.88	0.30	1.29	4.36
		1962-71	1998-2003		62-71	98-03	
Jan-Feb CUI	45 N	-59.35 ± 9.44	-110.50 ± 25.65	-38.95	2438	3948	1.62
Jan-Feb CUI	42 N	-40.25 ± 10.60	-101.08 ± 27.91	-60.83	1122	4674	4.16
Jan-Feb MEI		-0.26 ± 0.27	0.11 ± 0.60	0.37	0.90	1.47	1.63
Jan-Feb PDO		-0.65 ± 0.22	0.24 ± 0.49	0.89	0.48	1.45	3.02

Table 2. Halocline nutrient concentrations and nitrate-to-phosphate ratios for LTOP and TENOC for data shown in Figs. 18 and 19. Means ± SE are given for data sets grouped by halocline temperature. The warm halocline group has temperatures above the mean value of 9.2°C, and the cold halocline group has temperatures less than 9.2°C.

	Warm Halocline (≥ 9.2 °C)		
	NO_3^-	PO_4^{-3}	N:P
LTOP	12.16±0.84	1.28±0.04	9.44±0.54
TENOC	11.44±0.65	1.20±0.06	9.74±0.56

	Cool Halocline (< 9.2 °C)		
	NO_3^-	PO_4^{-3}	N:P
LTOP	18.52 ±0.95	1.65±0.08	11.25±0.29
TENOC	15.72±0.60	1.34±0.04	11.69±0.29

	Cool Halocline (< 9.2 °C, but omitting 2002-2003 data)		
	NO_3^-	PO_4^{-3}	N:P
LTOP	17.18±1.10	1.50±0.99	11.43±0.22
TENOC	15.72±0.60	1.34±0.04	11.69±0.29

LIST OF FIGURES

location and time-of-year of samples. Ticks on time axes mark the beginning of each month.

Figure 5. Seasonal cycle of sea level anomalies along 44.6°N calculated from 13 years (1993-2005) of altimeter data within the area between 44.1° and 45.1°N and between the coast and 132°W (a, *top*) without first removing the spatial mean, and (b, *bottom*) after removal of the spatial mean. Only the portion east of 130°W is shown. Alongtrack data from all available altimeters are used in the gridding (2-4 altimeters, depending on the period), as are data from the coastal tide gauge at Newport (Strub and James, 2002). Ticks on time axes mark the middle of each month. Dashed line indicates the offshore end of the NH line.

Figure 6. TENOC and LTOP seasonal cycles of 150 m temperature, 150 m salinity, and the geopotential anomaly at 150 m relative to 500 dbar. Contour intervals are 0.2°C, 0.05 psu and 0.1 J kg^{-1} (thin), and 1°C, 0.1 psu, and 0.2 J kg^{-1} (heavy). Small dots show location and time-of-year of samples. Ticks on time axes mark the beginning of each month.

Figure 7. TENOC and LTOP seasonal cycles of pressure (in decibars, equivalent to depth in meters) and temperature (°C) of the surface on which salinity is 33.0 psu. Data from stations less than 10 nm from the coast are excluded because this isohaline usually intersects the sea surface (in summer) or the shelf bottom (in winter). Small dots show location and time-of-year of samples. Ticks on time axes mark the beginning of each month.

Figure 8. Comparison of TENOC and LTOP summer sections: (a) TENOC temperature average (b) LTOP temperature average, (c) LTOP minus TENOC temperature difference, (d) TENOC salinity average (e) LTOP salinity average, (f) LTOP minus TENOC salinity difference. Colored contours in the difference panels (c, f) indicate the 95% (dotted) and 99% (dashed) significance levels.

Figure 9. Comparison of TENOC and LTOP winter sections: (a) TENOC temperature average, (b) LTOP temperature average, (c) average temperature difference (LTOP minus TENOC), (d) temperature variance ratio (LTOP/TENOC), (e) TENOC salinity average, (f) LTOP salinity average, (g) average salinity difference (LTOP minus TENOC), and (h) salinity variance ratio

(LTOP/TENOC). Differences and ratios were computed only for locations with at least three observations in each period.

Figure 10. Vertical profiles of average differences between LTOP and TENOC at NH-85, calculated from all available data regardless of season: (a) temperature, (b) salinity, and (c) density. Error bars represent 95% confidence intervals of the differences (calculated from t-test).

Figure 11. Individual profiles of LTOP steric heights compared to the TENOC average with standard deviations: (a, *left*) summer, (b, *right*) winter. Also shown for each season are the LTOP and TENOC averages, each with standard errors. A steric height change of 1 J kg^{-1} corresponds to a sea level change of 10 cm.

Figure 12. LTOP velocity averages for summer (upper row) and winter (lower row): geostrophic velocity relative to 500 dbar (left); measured northward current (center); and eastward measured current (right). Units are cm s^{-1}. Measured current averages were calculated from data for seven summers (1997-2003) and five winters (1998, 2000-2003).

Figure 13(a). Anomalies of dynamic height (geopotential anomaly, in J kg^{-1}) at the sea surface relative to 500 dbar, during TENOC and LTOP, plotted as a function of longitude and time. Large ticks on time axes mark the beginning of each year. Time series of the Multivariate ENSO Index (MEI) are shown for both periods.

Figure 13(b). Anomalies of dynamic height (geopotential anomaly, in J kg^{-1}) at 150 m relative to 500 dbar during TENOC and LTOP, plotted as a function of longitude and time. Large ticks on time axes mark the beginning of each year. Time series of the Multivariate ENSO Index (MEI) are shown for both periods.

Figure 14(a) Temperature on (°C) surface at which salinity is 33.0 psu during TENOC and LTOP, , plotted as a function of longitude and time. Large ticks on time axes mark the beginning of each year. Time series of the Multivariate ENSO Index (MEI) are shown for both periods.

Figure 14. Pressure (in dbar, equivalent to depth in meters) on the surface at which salinity is 33.0 psu, plotted as a function of longitude and time. Large ticks on time axes mark the beginning of each year. Time series of the Multivariate ENSO Index (MEI) are shown for both periods.

Figure 15. Nitrate concentrations (mmol m^{-3}) measured during LTOP: (a, *left*) at 10 m depth, and (b, *right*) on the 33.0 isohaline, plotted as a function of longitude and time. The white mask inshore indicates times when this isohaline intersects the sea surface or the bottom (gray squares). Large ticks on time axes mark the beginning of each year.

Figure 16. Chlorophyll concentrations in the surface layer during LTOP: (a, *left*) measured at 10 m depth on LTOP surveys: (b, *right*) estimated from SeaWiFS satellite data. The SeaWiFS values are 8-day composites with 4 km resolution; white areas represent missing values due to cloud cover. Large ticks on time axes mark the beginning of each year.

Figure 17. Seasonal cycle of (a, *left*) chlorophyll from SeaWiFS, and (b, *right*) of copepod biomass (line) and diversity (bars, mean +/- SE) at NH-5 over the inner shelf (from Hooff and Peterson, 2006). Copepod climatology is based on data from 1996-2004. Large ticks on time axes mark the beginning of each year.

Figure 18. Time series of ocean parameters during LTOP, with coho survival and climate indices. Top to bottom: hatchery coho survival (OPIH) by smolt year from the Oregon Department of Fish and Wildlife; vertically integrated and horizontally averaged chlorophyll concentration from the GLOBEC LTOP surveys, with bars showing ±1 standard deviation; phosphate in the halocline at NH-25 (at S = 33 psu); nitrate in the halocline at NH-25 (at S = 33 psu); halocline temperature at NH-25 (at S = 33); vertical shear of the measured alongshore northward current at NH-10 ($v_{10} - v_{60}$); monthly anomalies of the coastal upwelling index at 45°N; adjusted sea level anomalies at Crescent City (41.9°N); monthly shore temperature anomalies at Amphritite Pt (48.5°N); the Pacific Decadal Oscillation; and the multivariate ENSO index. Large ticks on time axes mark the beginning of each year.

Figure 19. Time series of ocean parameters during TENOC, with coho survival and climate indices. Top to bottom: hatchery coho survival (OPIH) by smolt year from Emlen *et al*. (1990); phosphate in the halocline (at S=33 psu); nitrate in the halocline (at S=33 psu); halocline temperature at NH-25 (S = 33 psu); vertical shear of the geostrophic current at NH-10 ($v_0 - v_{30}$); monthly anomalies of the

coastal upwelling index at 45°N; adjusted sea level anomalies at Crescent City (41.9°N) ; monthly shore temperature anomalies at Amphritite Pt. (48.5°N); the Pacific Decadal Oscillation; and the multivariate ENSO index. Large ticks on time axes mark the beginning of each year.

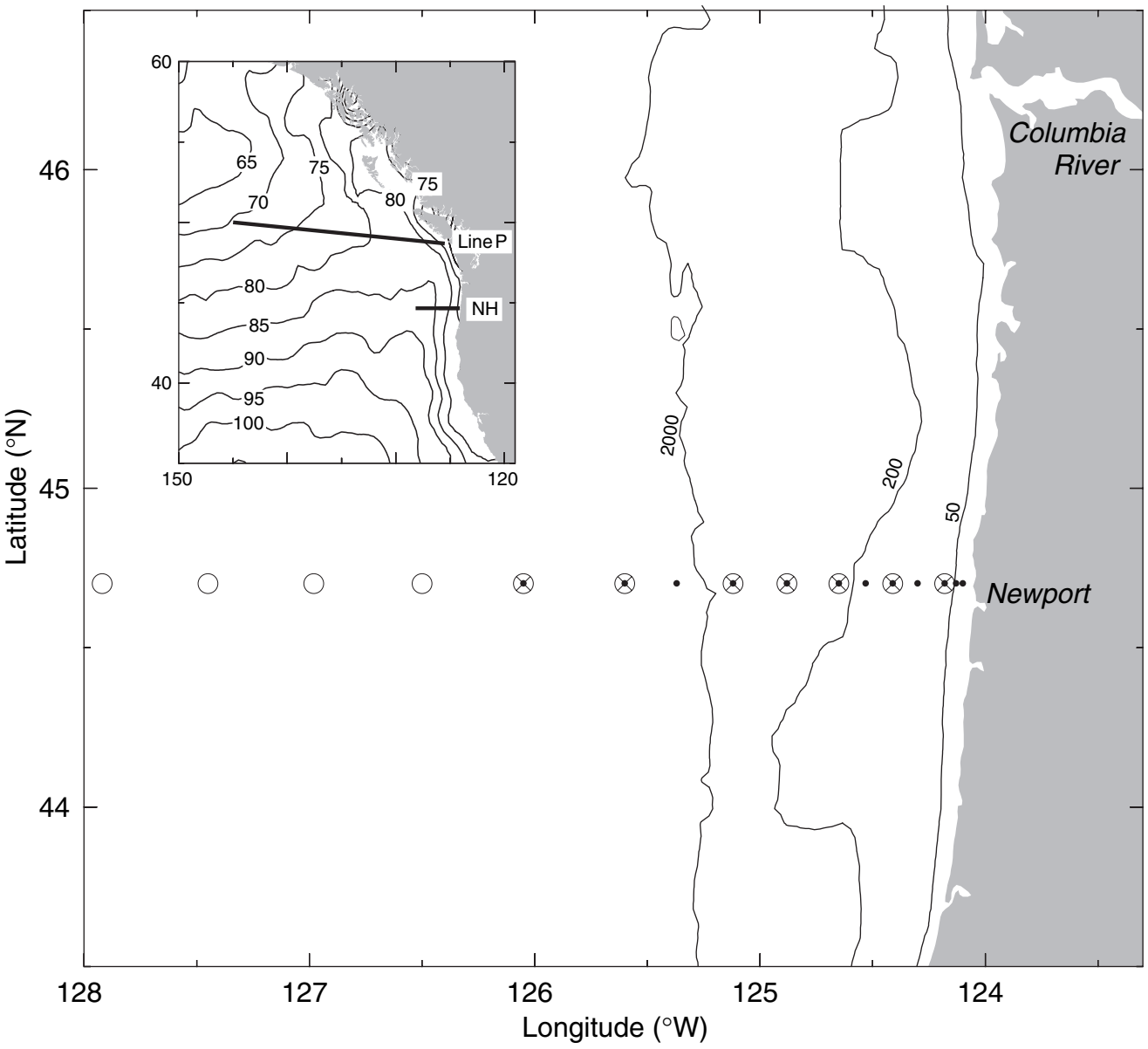
60
40
150
120
65
70
75
80
85
90
95
100
75
80
Line P
NH
2000
200
50
Columbia
River
Newport
46
45
44
Latitude (°N)
128
127
126
125
124
Longitude (°W)

Figure 1

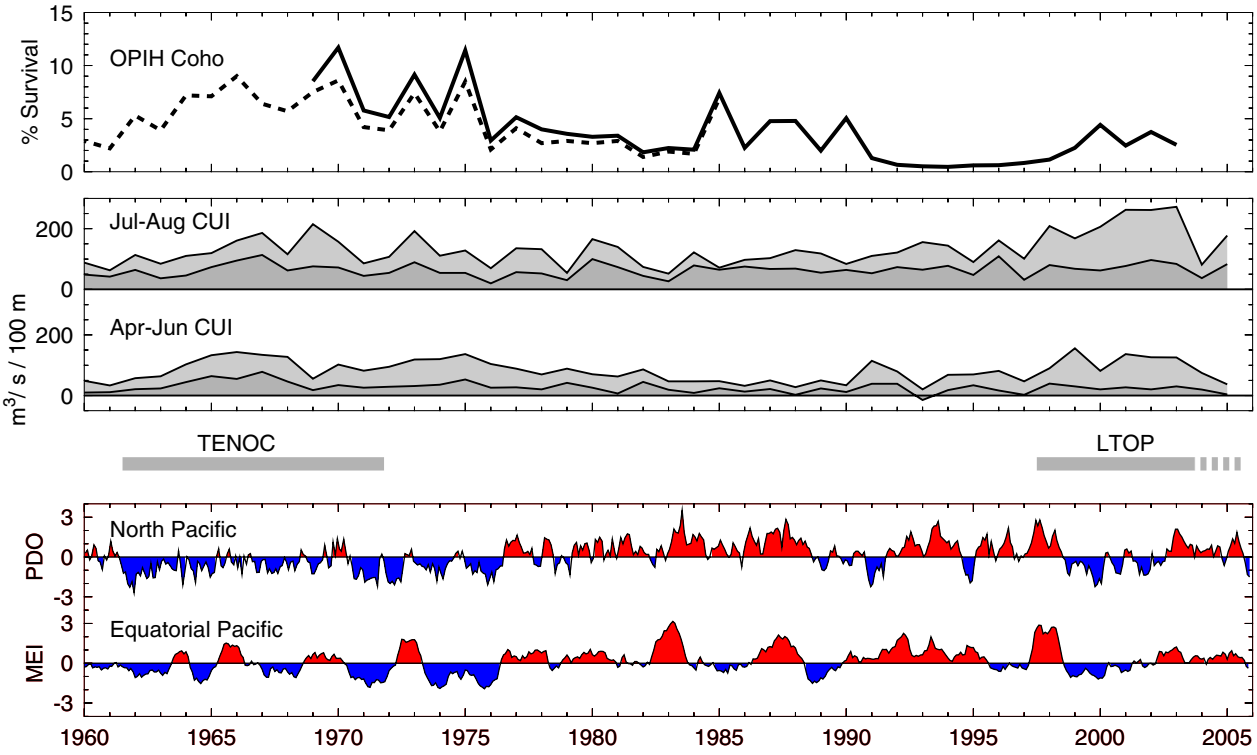
% Survival
OPIH Coho
Jul-Aug CUI
Apr-Jun CUI
m3/ s / 100 m
TENOC
LTOP
PDO
North Pacific
MEI
Equatorial Pacific
1960
1965
1970
1975
1980
1985
1990
1995
2000
2005

Figure 2

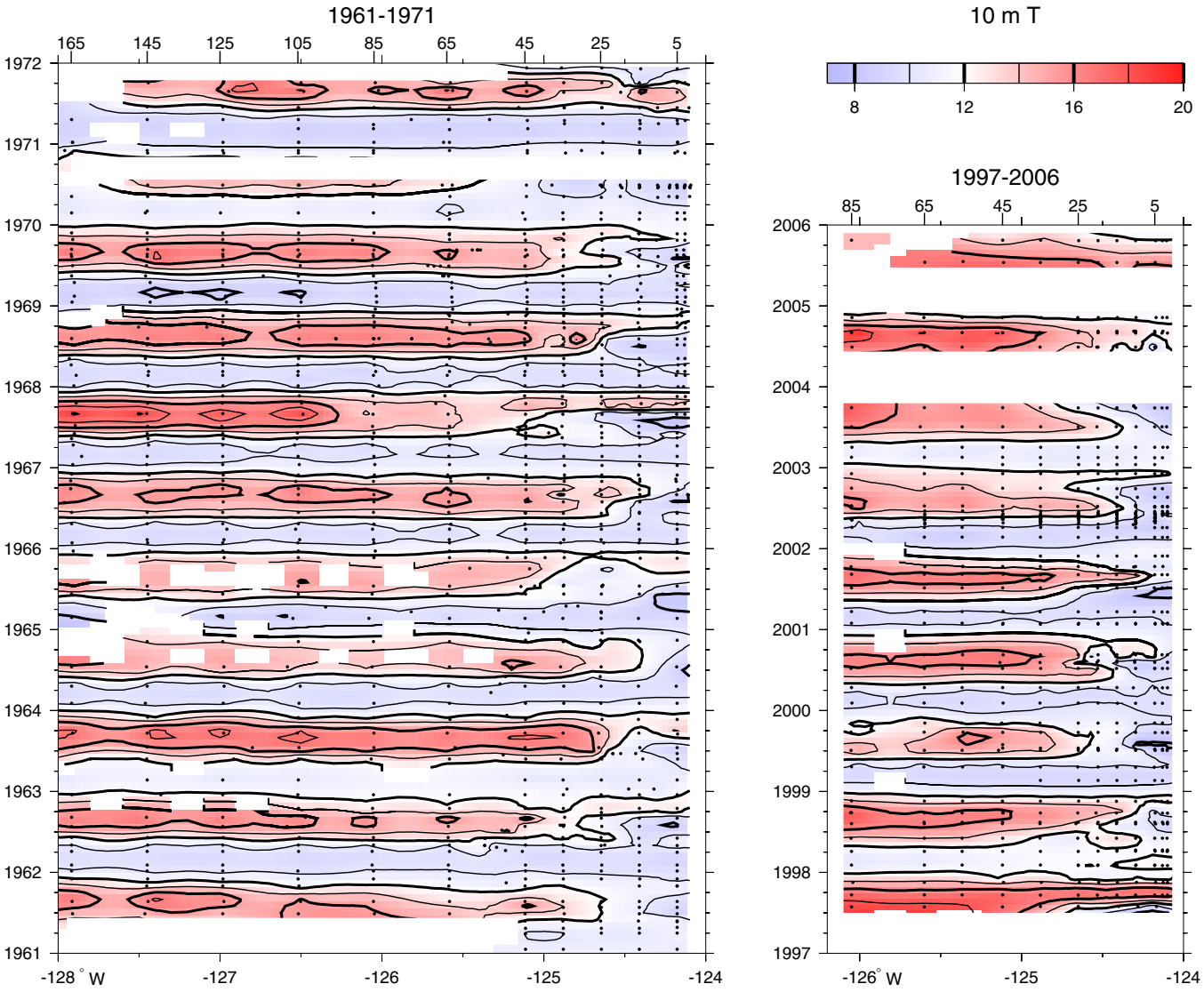
1961-1971
165
145
125
105
85
65
45
25
5
1972
1971
1970
1969
1968
1967
1966
1965
1964
1963
1962
1961
-128 ° W
-127
-126
-125
-124
10 m T
8
12
16
20
1997-2006
85
65
45
25
5
2006
2005
2004
2003
2002
2001
2000
1999
1998
1997
-126° W
-125
-124

Figure 3(a)

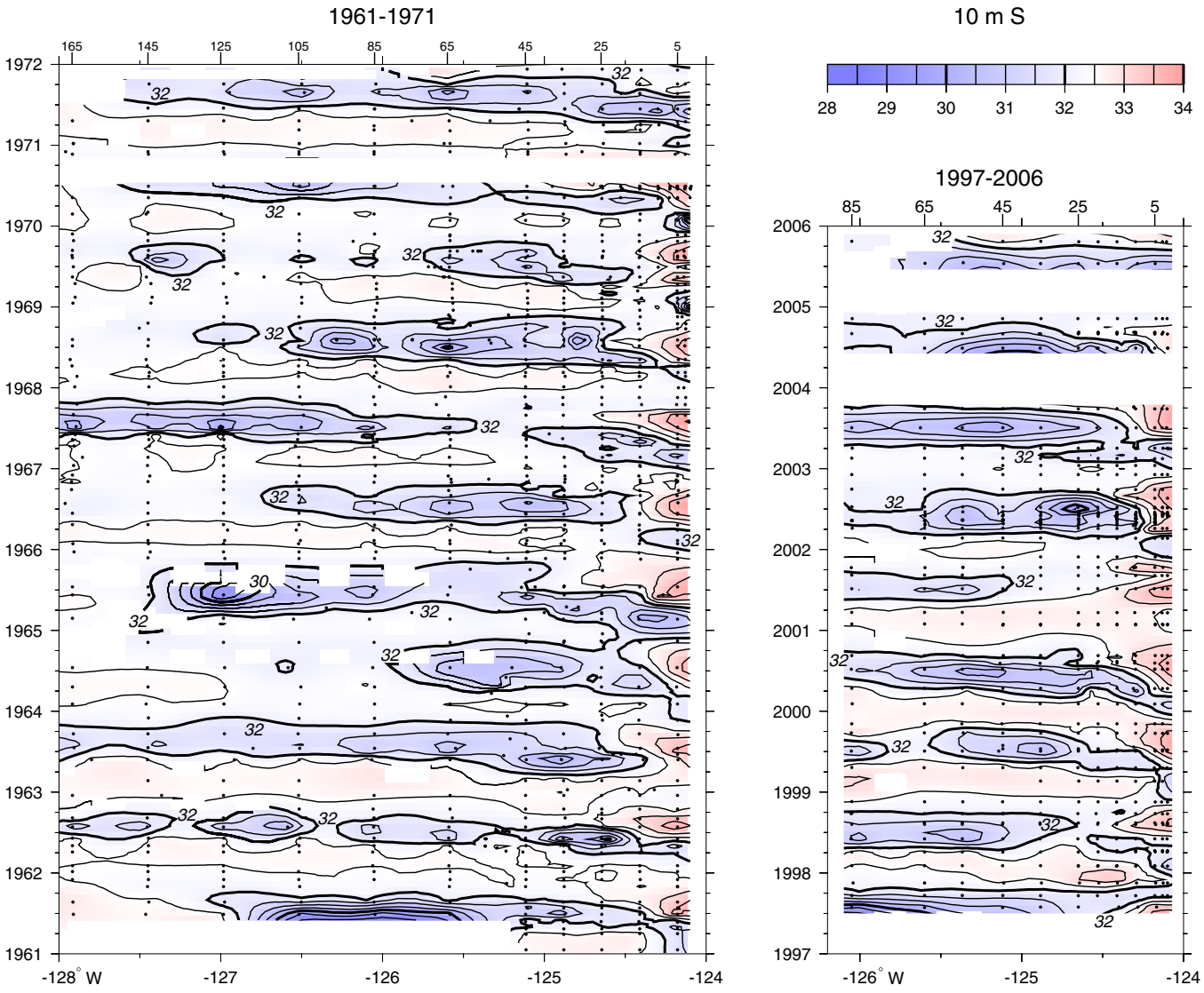
1961-1971
10 m S
28 29 30 31 32 33 34
1997-2006
165 145 125 105 85 65 45 25 5
85 65 45 25 5
1972 1971 1970 1969 1968 1967 1966 1965 1964 1963 1962 1961
2006 2005 2004 2003 2002 2001 2000 1999 1998 1997
32
30
-128° W -127 -126 -125 -124
-126° W -125 -124

Figure 3(b)

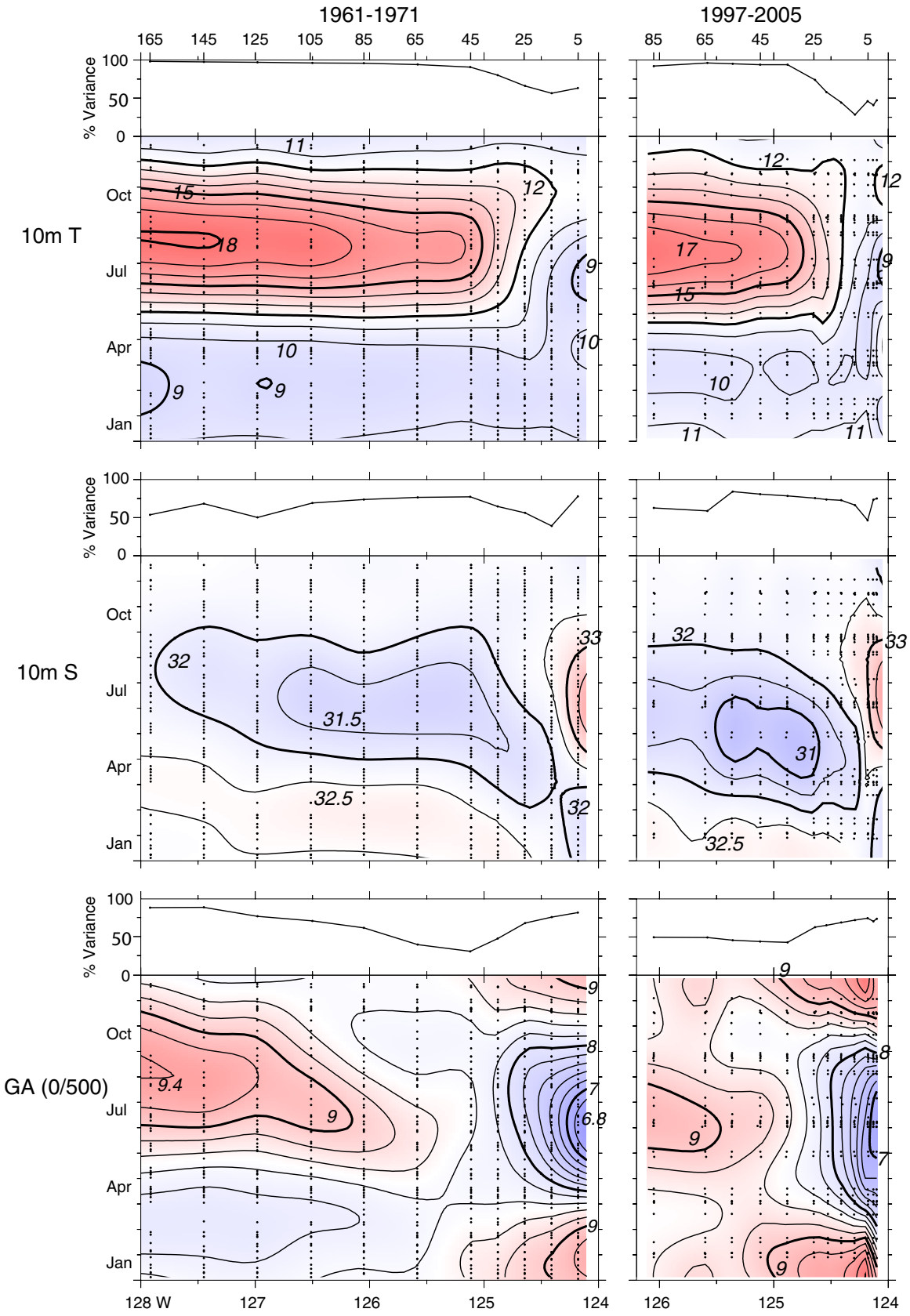
1961-1971
1997-2005
165
145
125
105
85
65
45
25
5
% Variance
100
50
0
Oct
Jul
Apr
Jan
10m T
10m S
GA (0/500)
11
12
15
18
9
10
17
31.5
32
32.5
33
31
9.4
8
7
6.8
128 W
127
126
125
124

Figure 4

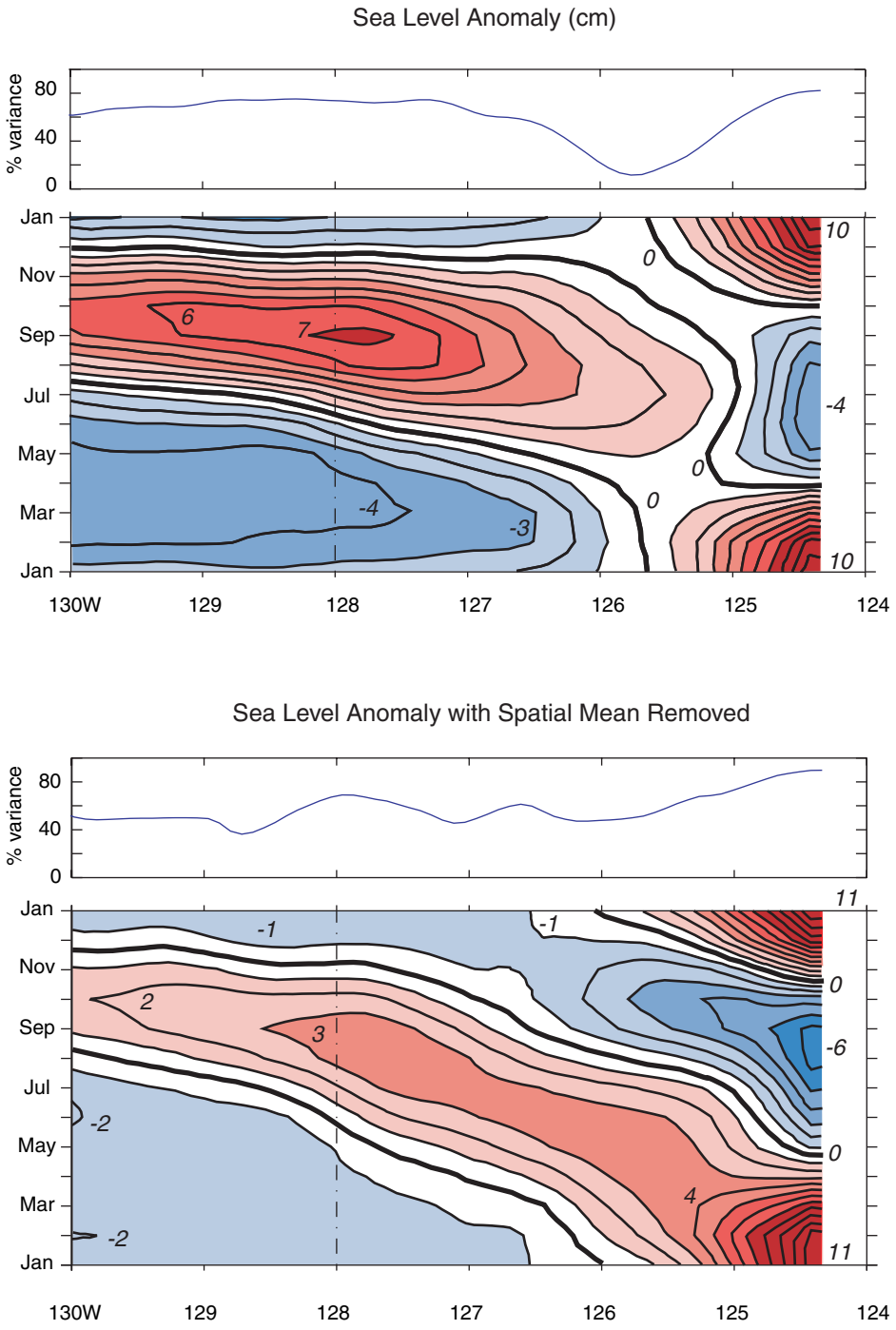
Sea Level Anomaly (cm)
% variance
80
40
0
Jan
Nov
Sep
Jul
May
Mar
Jan
6
7
-4
-3
0
0
0
10
-4
10
130W
129
128
127
126
125
124
Sea Level Anomaly with Spatial Mean Removed
% variance
80
40
0
Jan
Nov
Sep
Jul
May
Mar
Jan
-1
-1
2
3
-2
-2
4
11
0
-6
0
11
130W
129
128
127
126
125
124

Figure 5

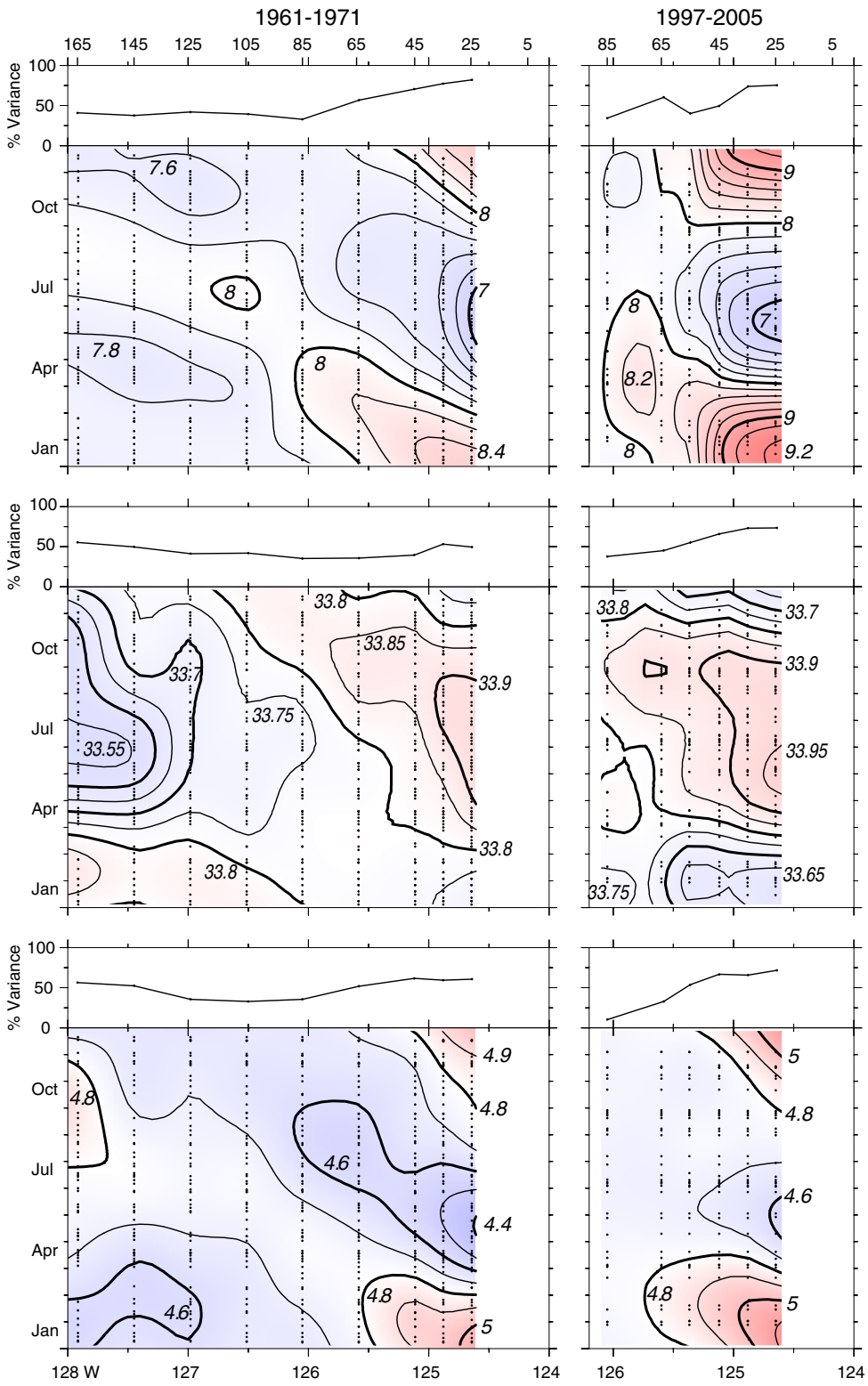

150m T

150m S

GA (150/500)

Figure 6

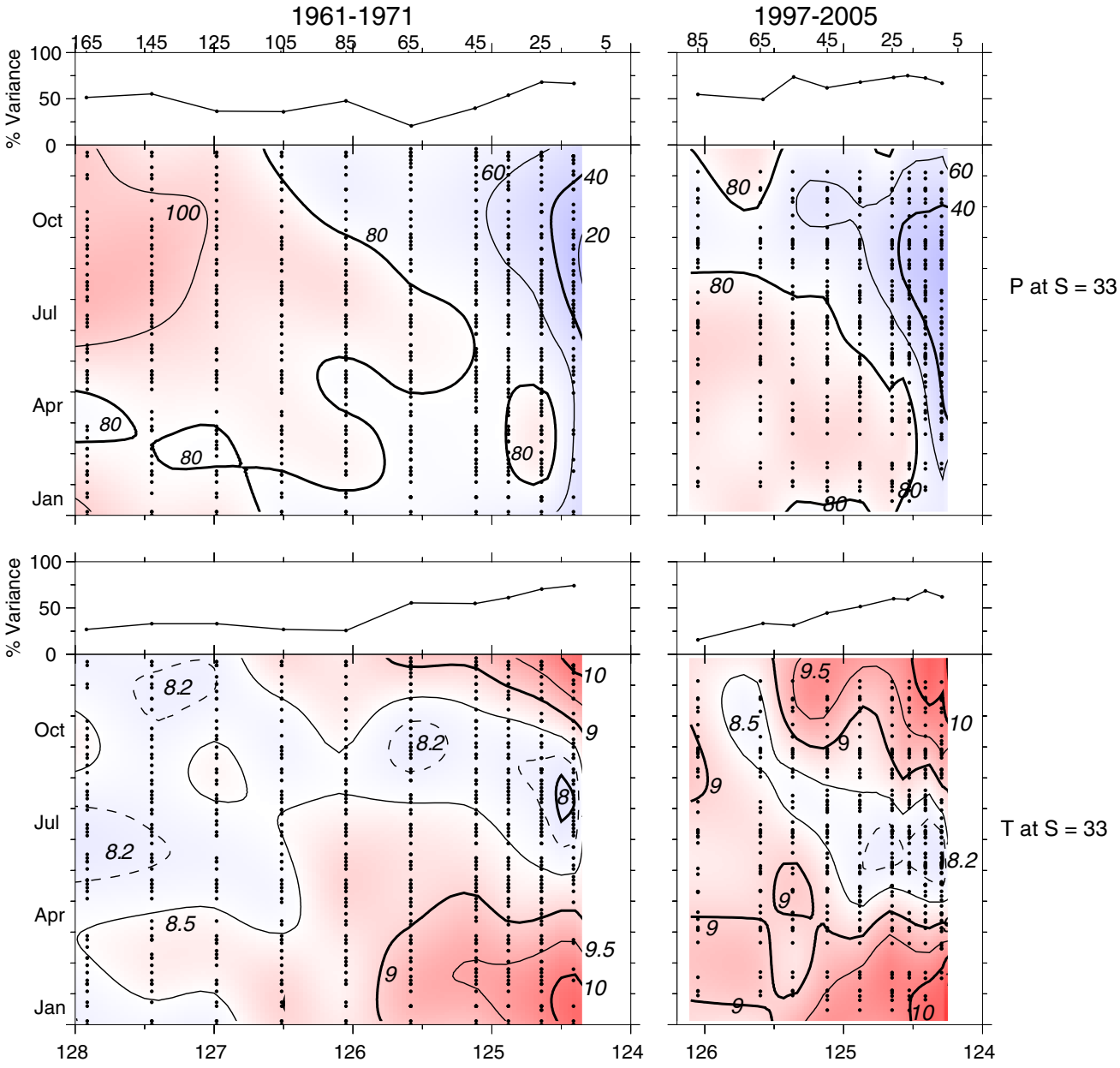
1961-1971
1997-2005
% Variance
100
50
0
165
145
125
105
85
65
45
25
5
Oct
Jul
Apr
Jan
100
80
60
40
20
P at S = 33
8.2
10
9
8.5
9.5
T at S = 33
128
127
126
125
124

Figure 7

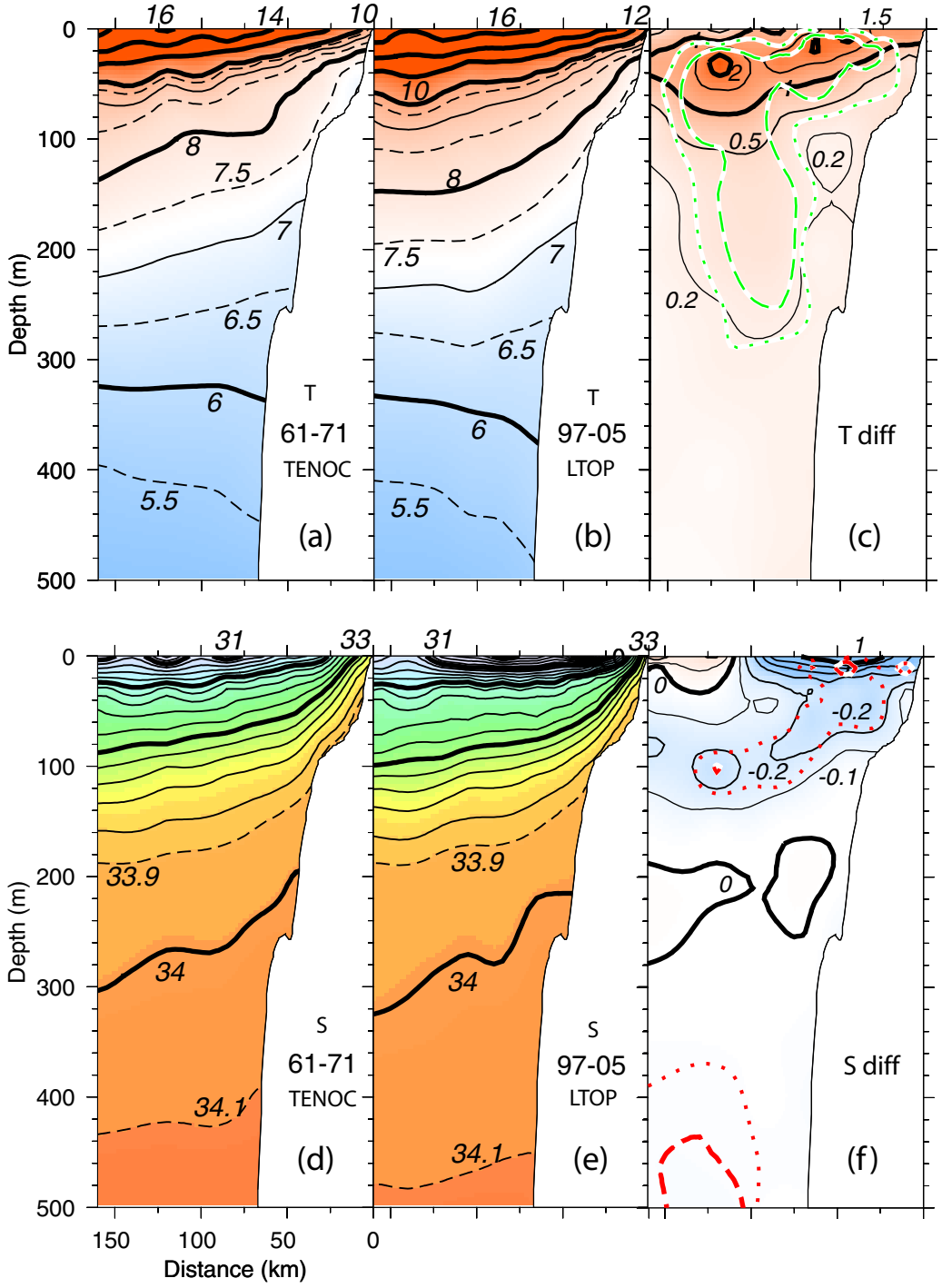
Depth (m)
0
100
200
300
400
500
16
14
10
8
7.5
7
6.5
6
5.5
T
61-71
TENOC
(a)
16
12
10
8
7.5
7
6.5
6
5.5
T
97-05
LTOP
(b)
1.5
2
0.5
0.2
0.2
T diff
(c)
31
33
33.9
34
34.1
S
61-71
TENOC
(d)
31
33
33.9
34
34.1
S
97-05
LTOP
(e)
1
0
-0.2
-0.2
-0.1
0
S diff
(f)
150
100
50
0
Distance (km)

Figure 8

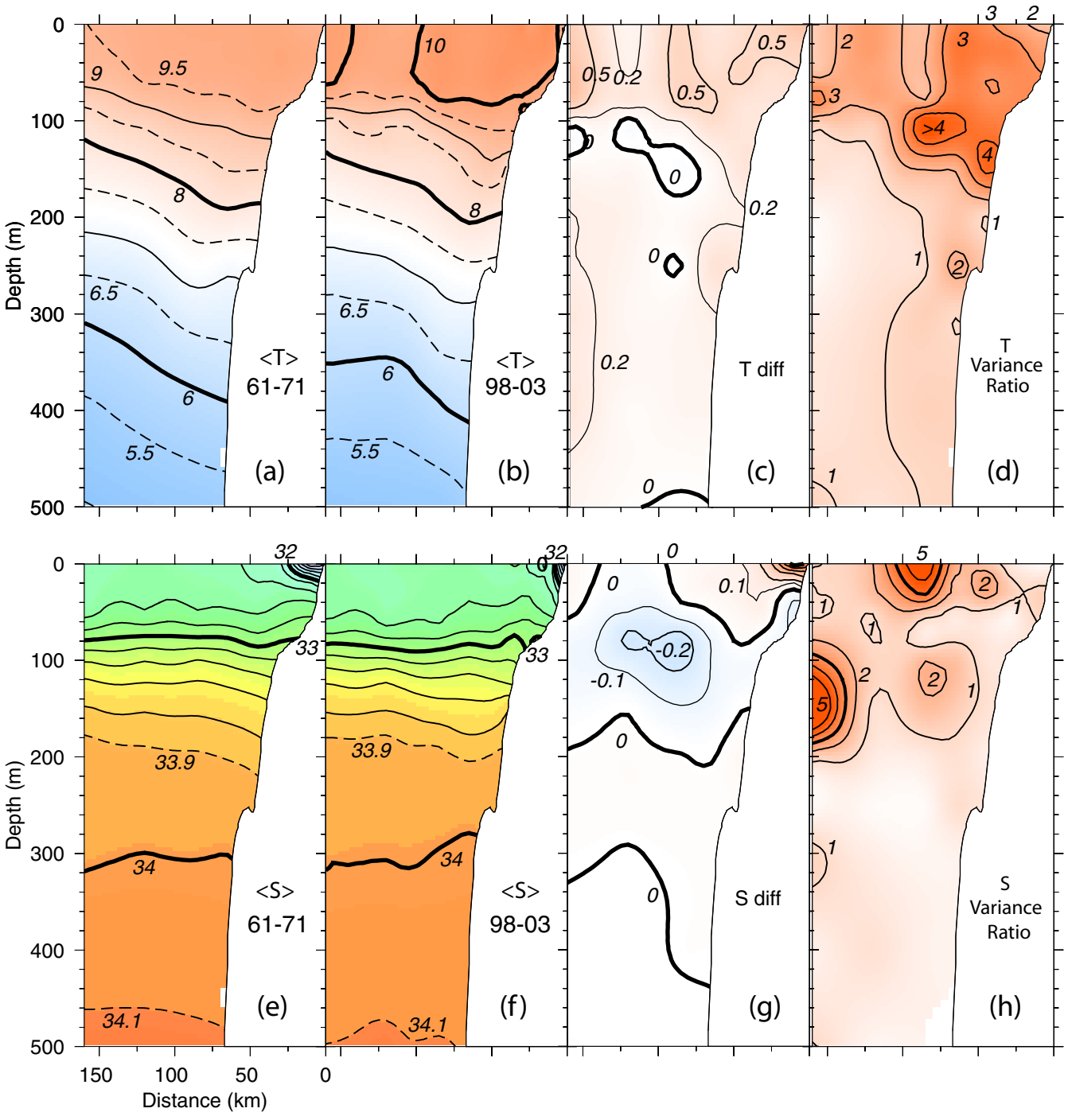
Depth (m)
0
100
200
300
400
500
<T>
61-71
(a)
<T>
98-03
(b)
T diff
(c)
T
Variance
Ratio
(d)
<S>
61-71
(e)
<S>
98-03
(f)
S diff
(g)
S
Variance
Ratio
(h)
150
100
50
0
Distance (km)

Figure 9

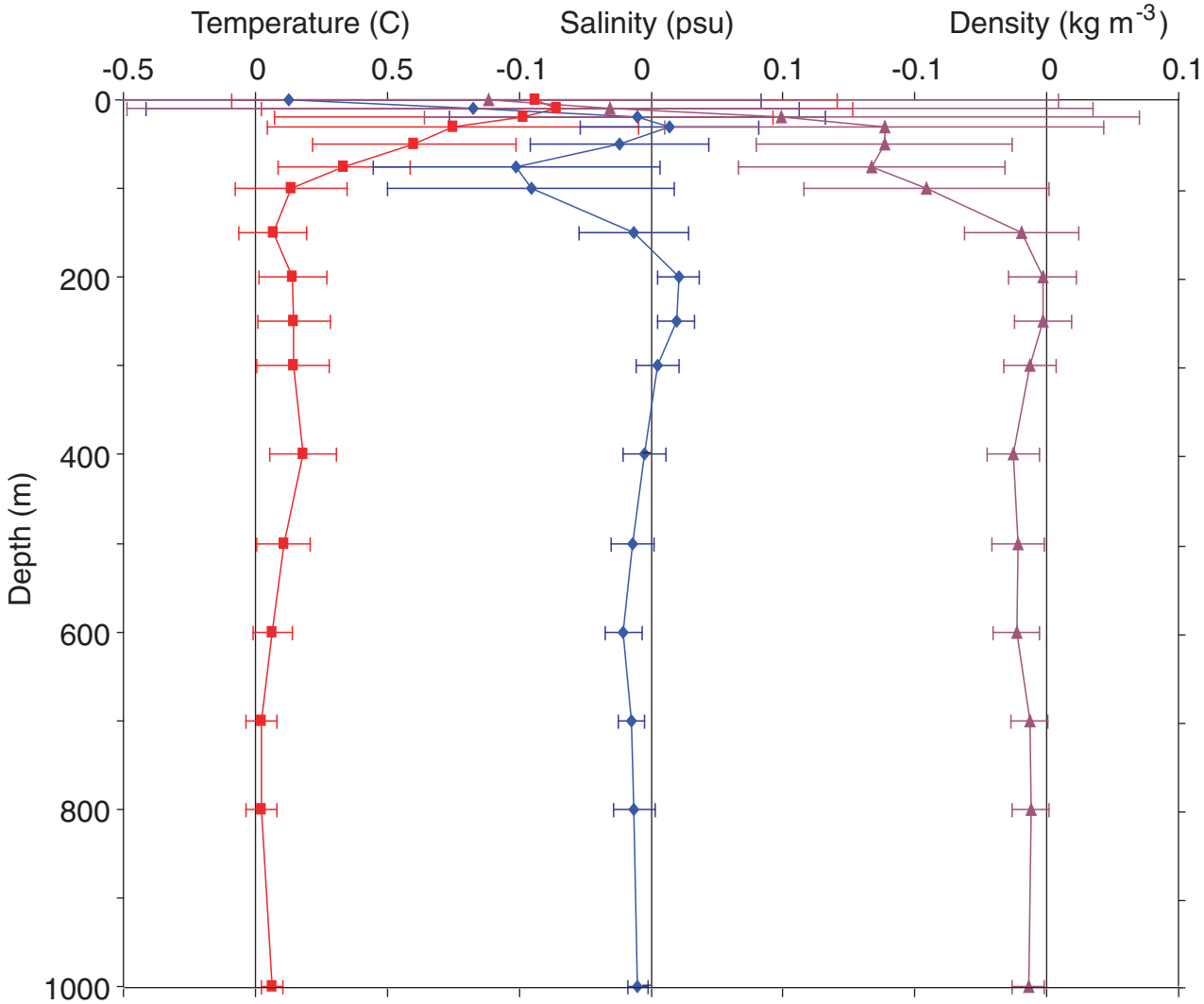
Temperature (C)
Salinity (psu)
Density (kg m-3)
-0.5
0
0.5
-0.1
0
0.1
-0.1
0
0.1
Depth (m)
0
200
400
600
800
1000

Figure 10

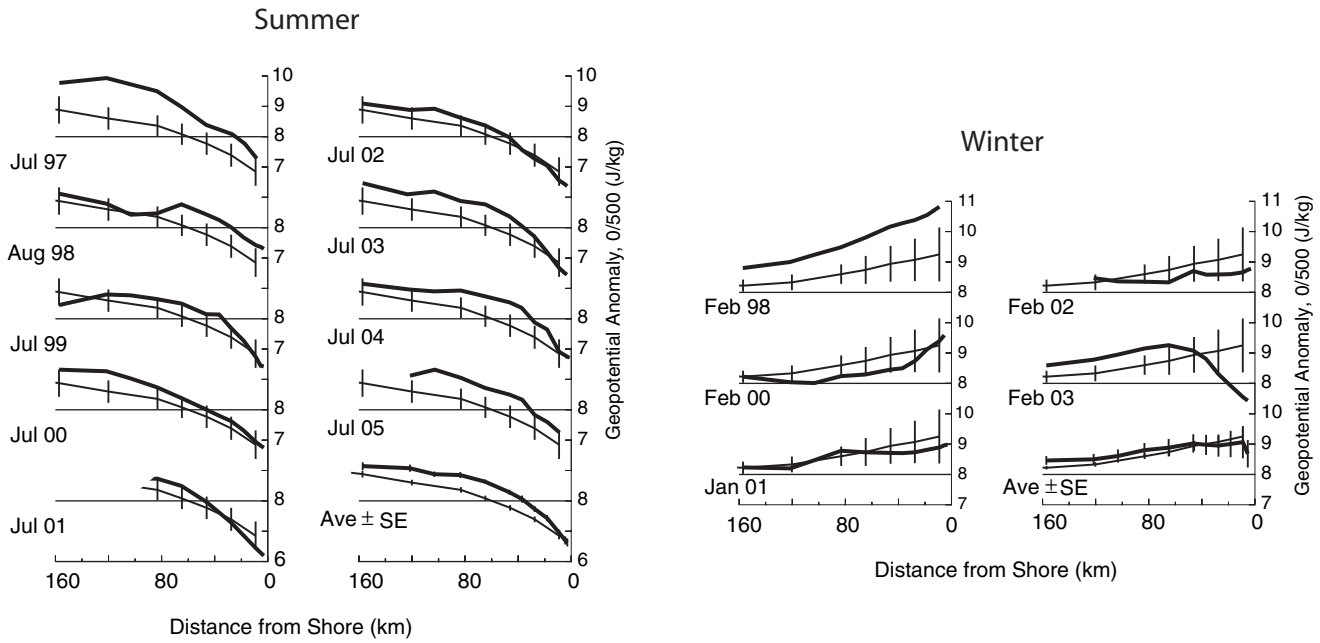
Summer
Jul 97
Aug 98
Jul 99
Jul 00
Jul 01
Jul 02
Jul 03
Jul 04
Jul 05
Ave ± SE
Geopotential Anomaly, 0/500 (J/kg)
Distance from Shore (km)
Winter
Feb 98
Feb 00
Jan 01
Feb 02
Feb 03
Ave ±SE
Geopotential Anomaly, 0/500 (J/kg)
Distance from Shore (km)

Figure 11

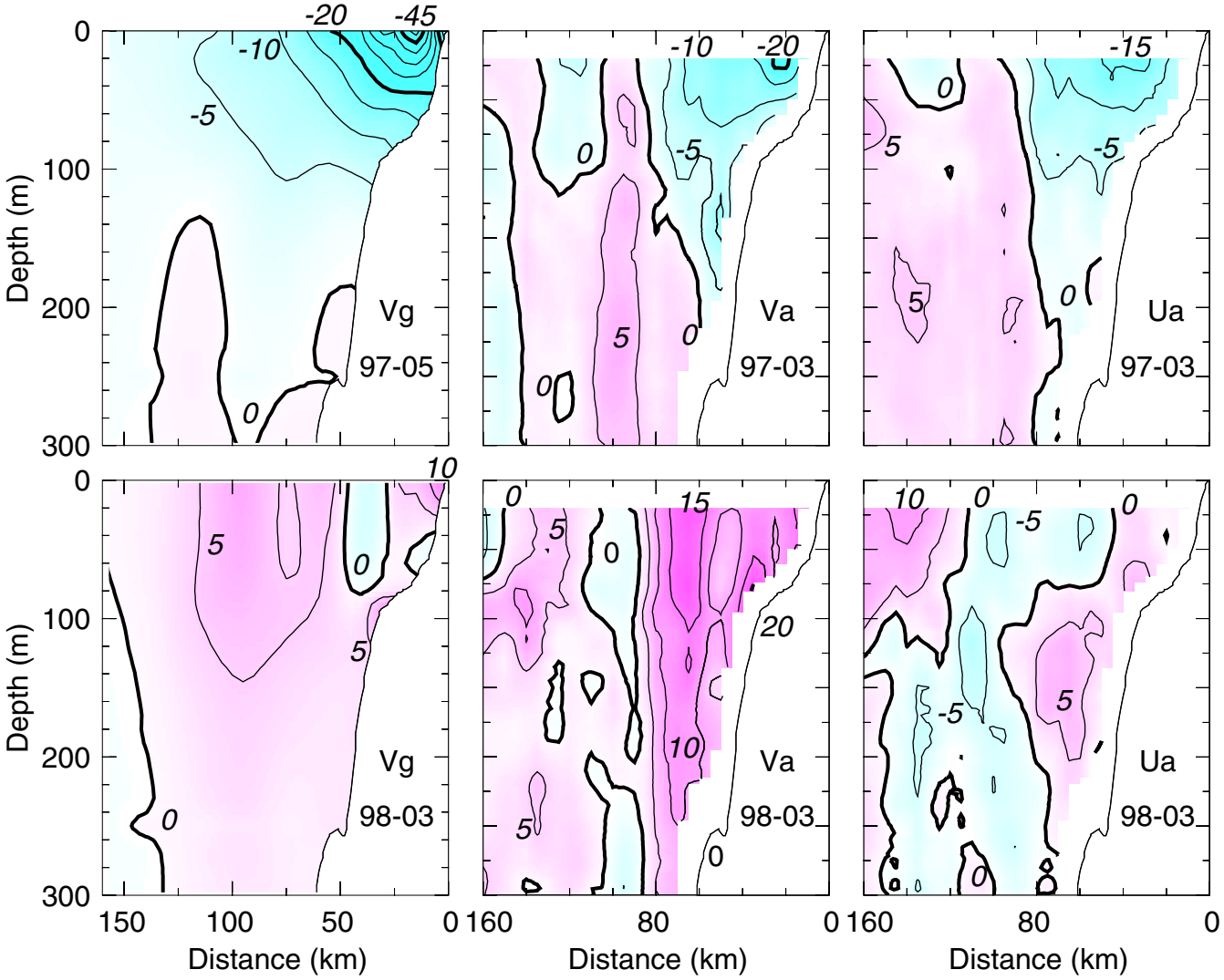
Depth (m)
0
100
200
300
Vg
97-05
Va
97-03
Ua
97-03
Vg
98-03
Va
98-03
Ua
98-03
150
100
50
0
160
80
0
Distance (km)

Figure 12

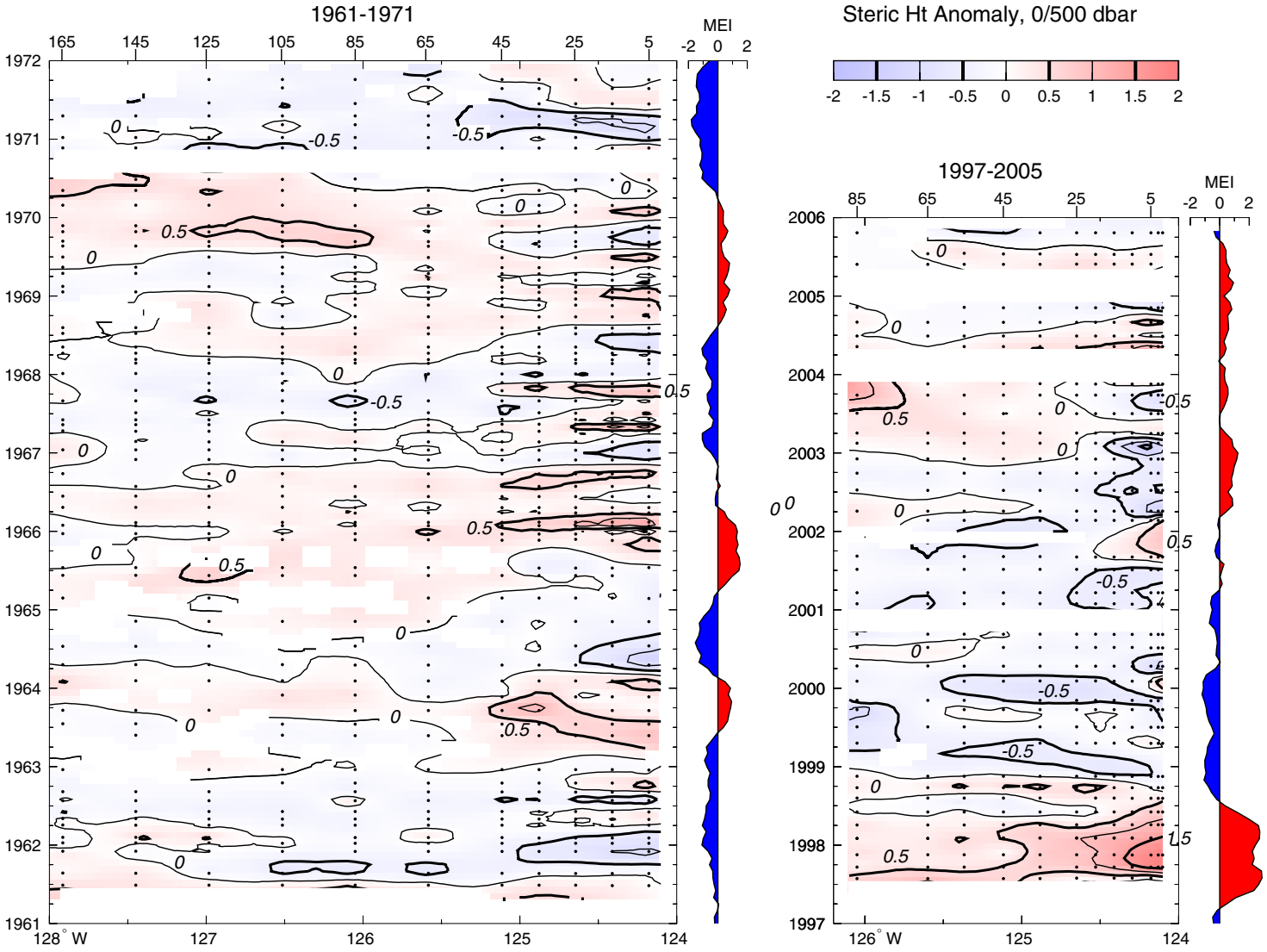
1961-1971
MEI
Steric Ht Anomaly, 0/500 dbar
-2 -1.5 -1 -0.5 0 0.5 1 1.5 2
1997-2005
MEI
128° W
127
126
125
124
126° W

Figure 13(a)

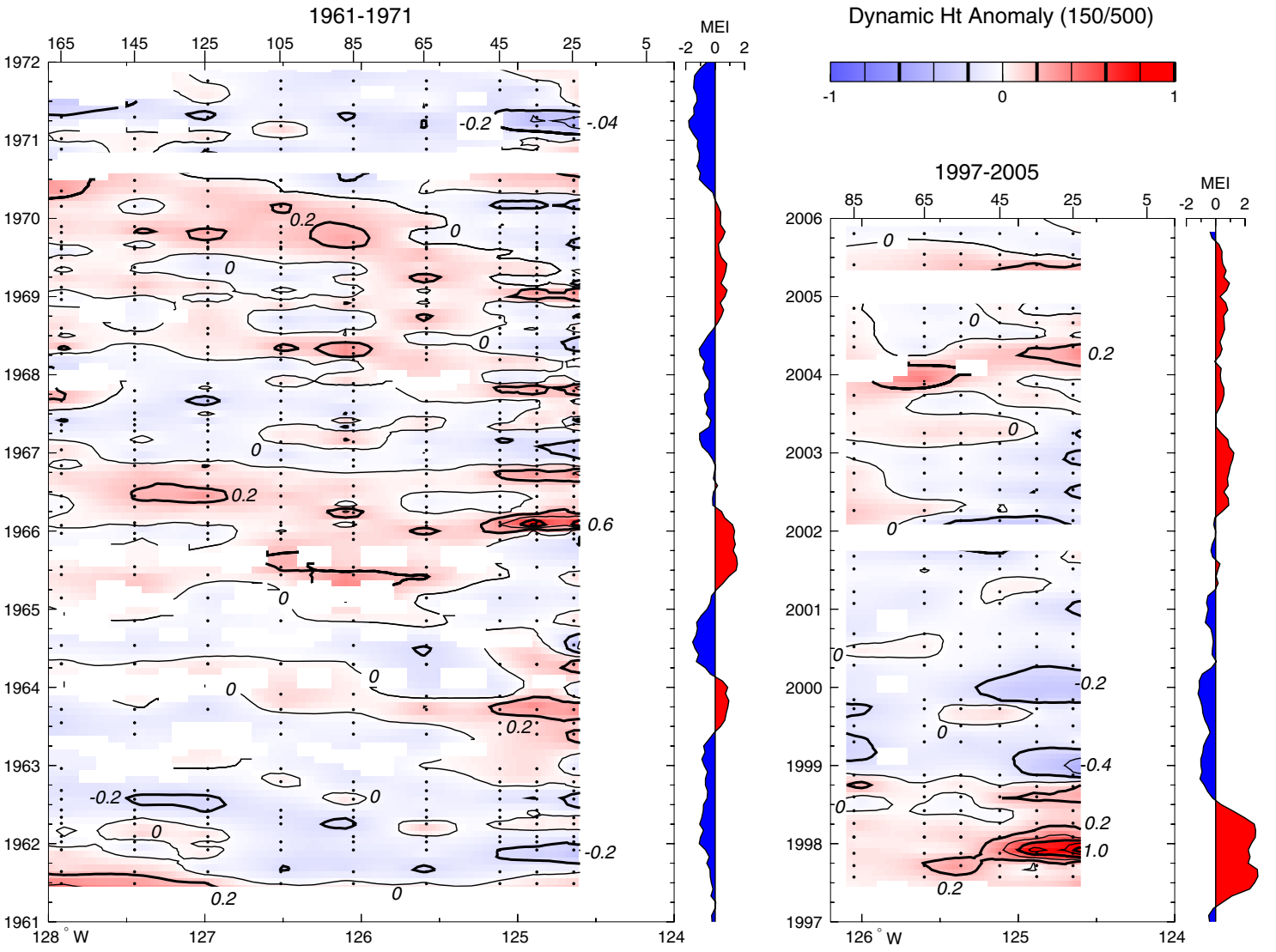
1961-1971
MEI
Dynamic Ht Anomaly (150/500)
1997-2005
MEI
128 ° W
127
126
125
124
126 ° W
125
124

Figure 13(b)

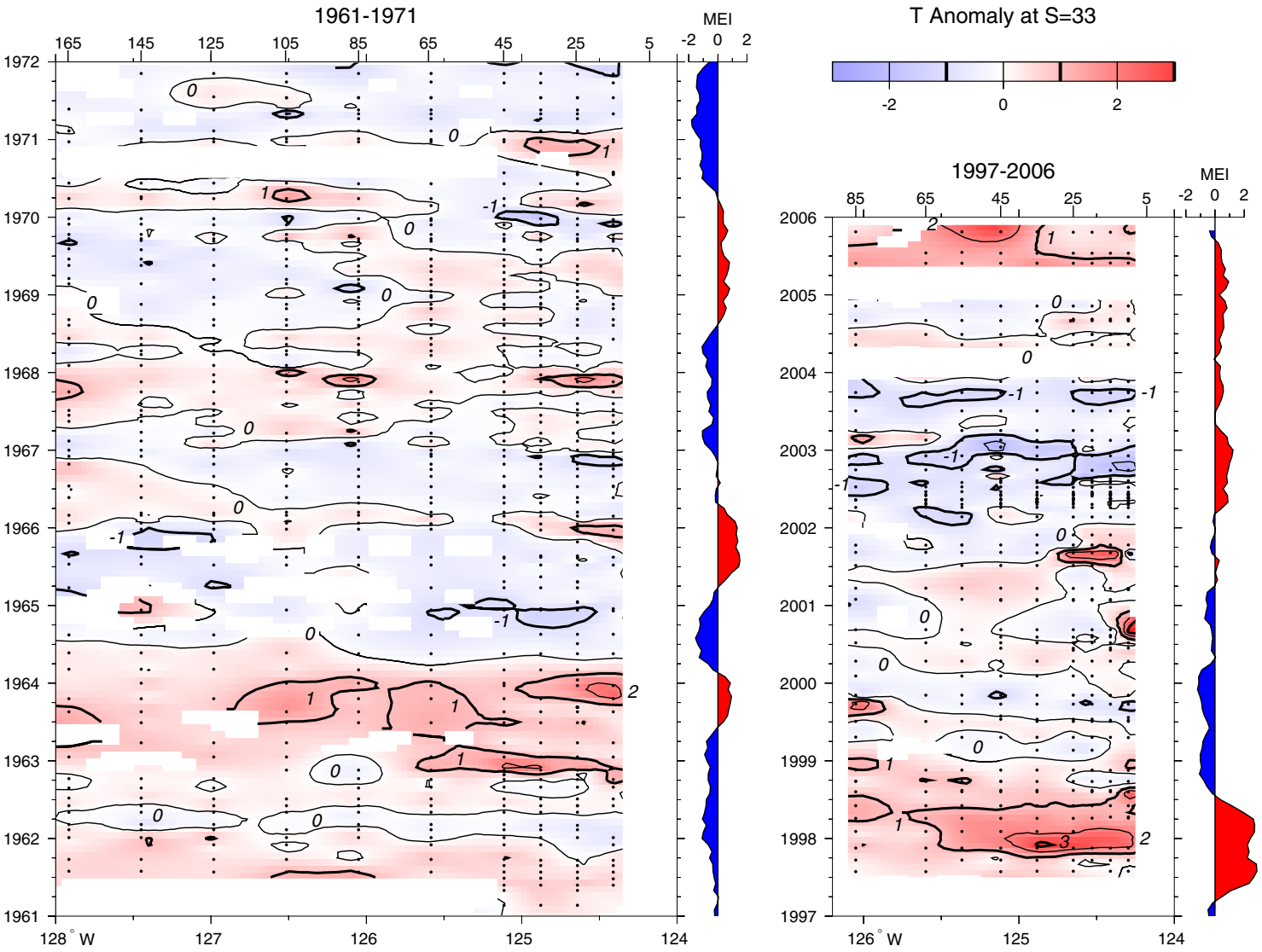
1961-1971
MEI
165 145 125 105 85 65 45 25 5
-2 0 2
1972 1971 1970 1969 1968 1967 1966 1965 1964 1963 1962 1961
128° W 127 126 125 124
T Anomaly at S=33
-2 0 2
1997-2006
MEI
85 65 45 25 5
-2 0 2
2006 2005 2004 2003 2002 2001 2000 1999 1998 1997
126° W 125 124

Figure 14(a)

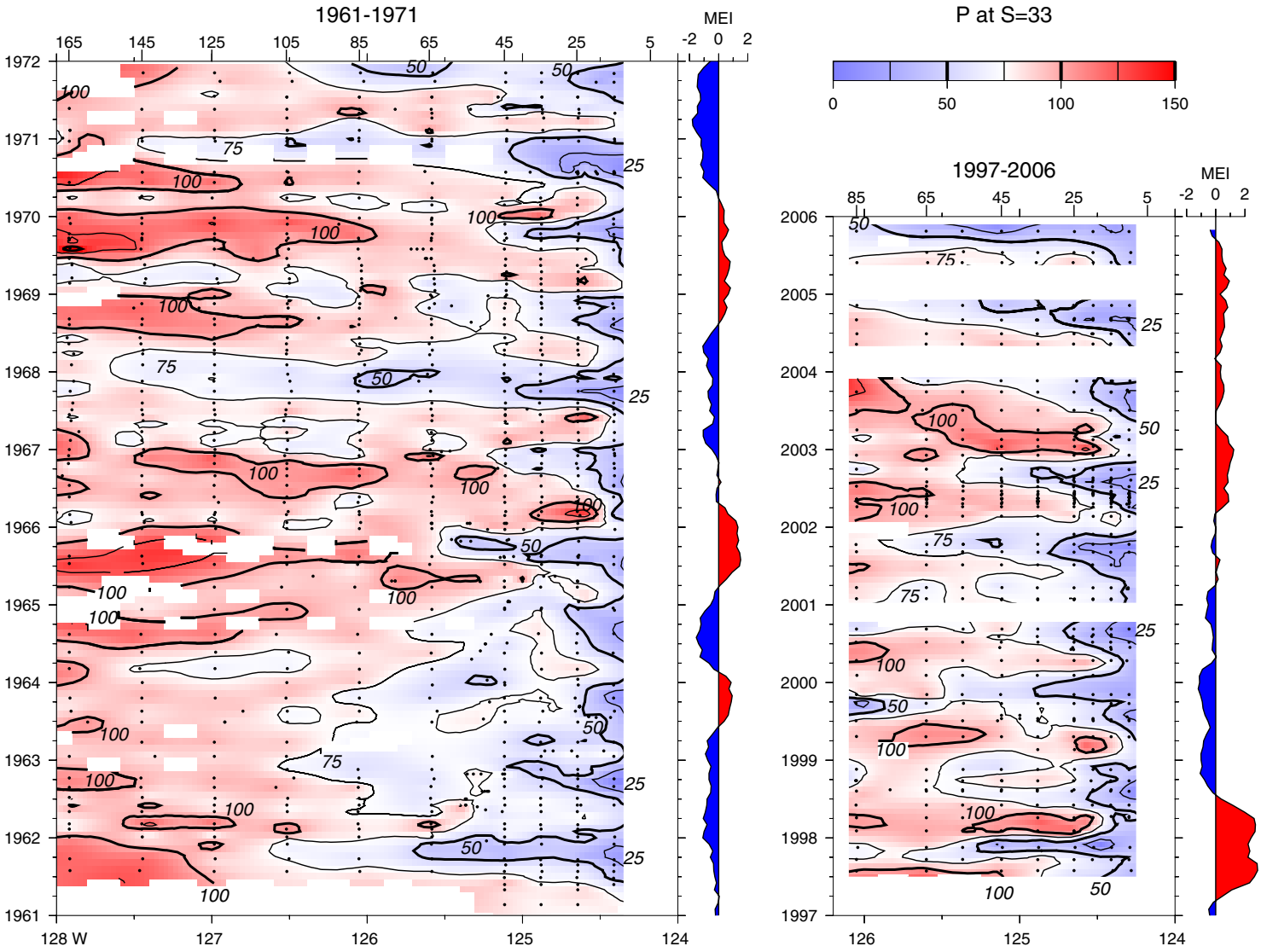

Figure 14(b)

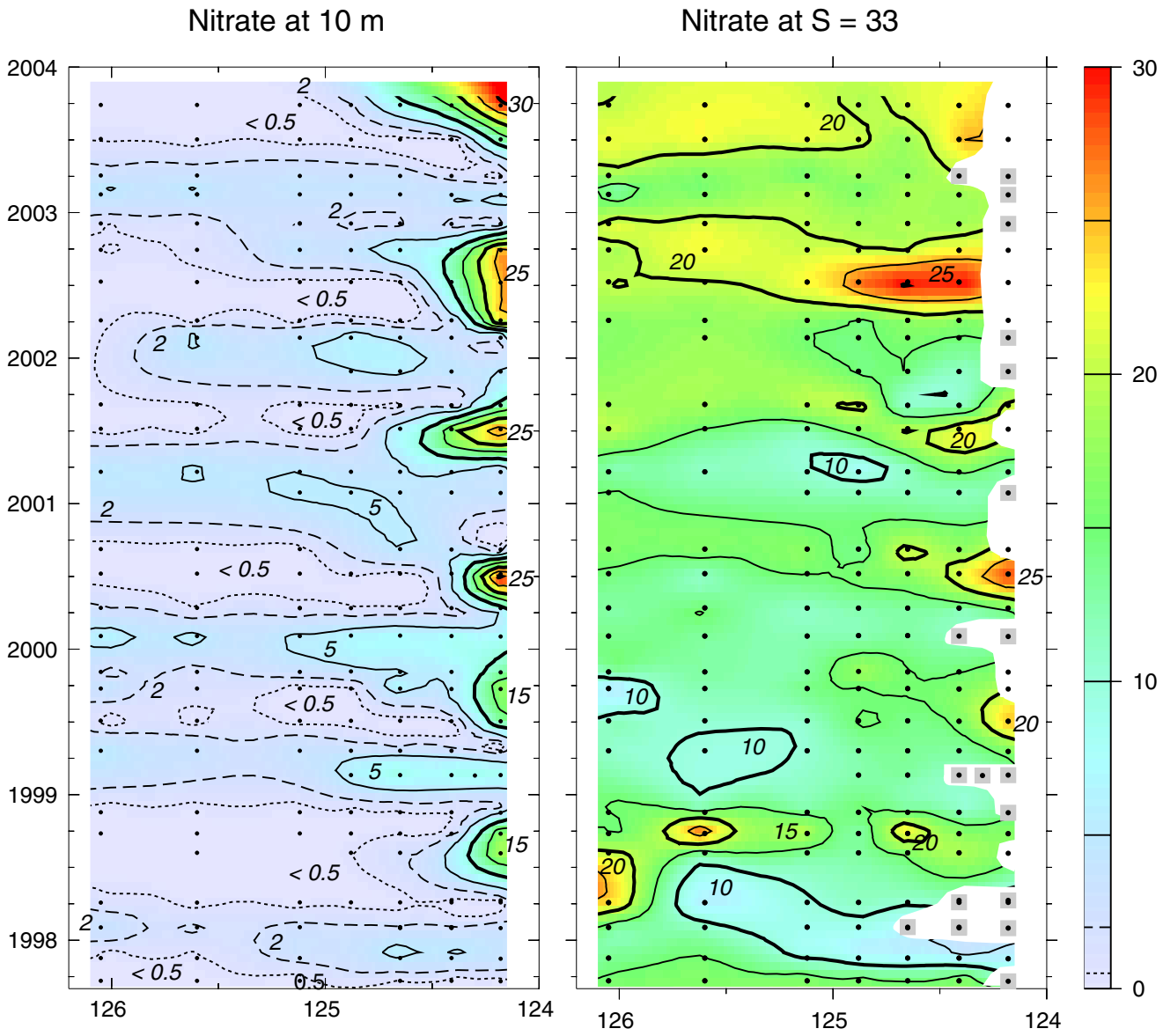
Nitrate at 10 m
Nitrate at S = 33
2004
2003
2002
2001
2000
1999
1998
126
125
124
30
25
20
15
10
5
2
< 0.5
0.5

Figure 15

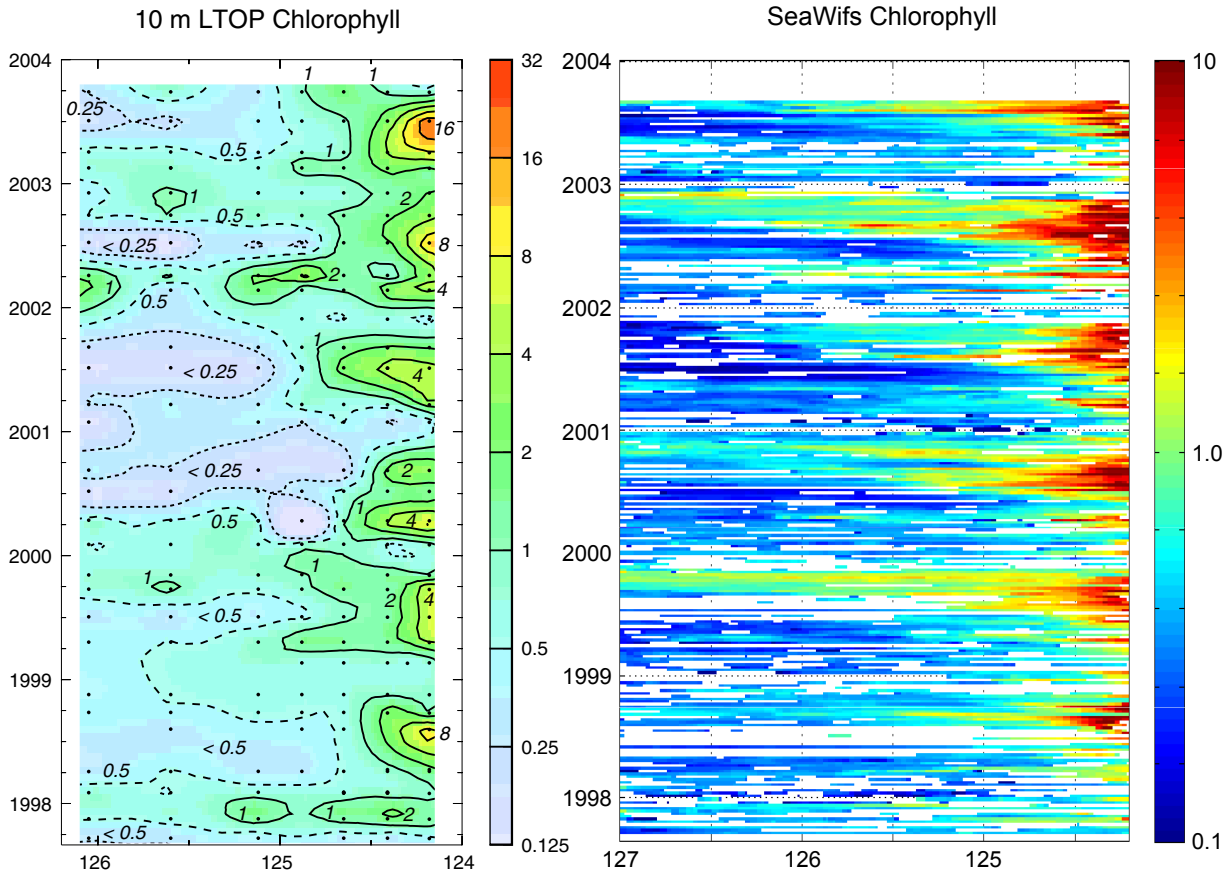
10 m LTOP Chlorophyll
SeaWifs Chlorophyll
2004
2003
2002
2001
2000
1999
1998
126
125
124
127
32
16
8
4
2
1
0.5
0.25
0.125
10
1.0
0.1
0.25
0.5
1
2
4
8
16
< 0.25
< 0.5

Figure 16

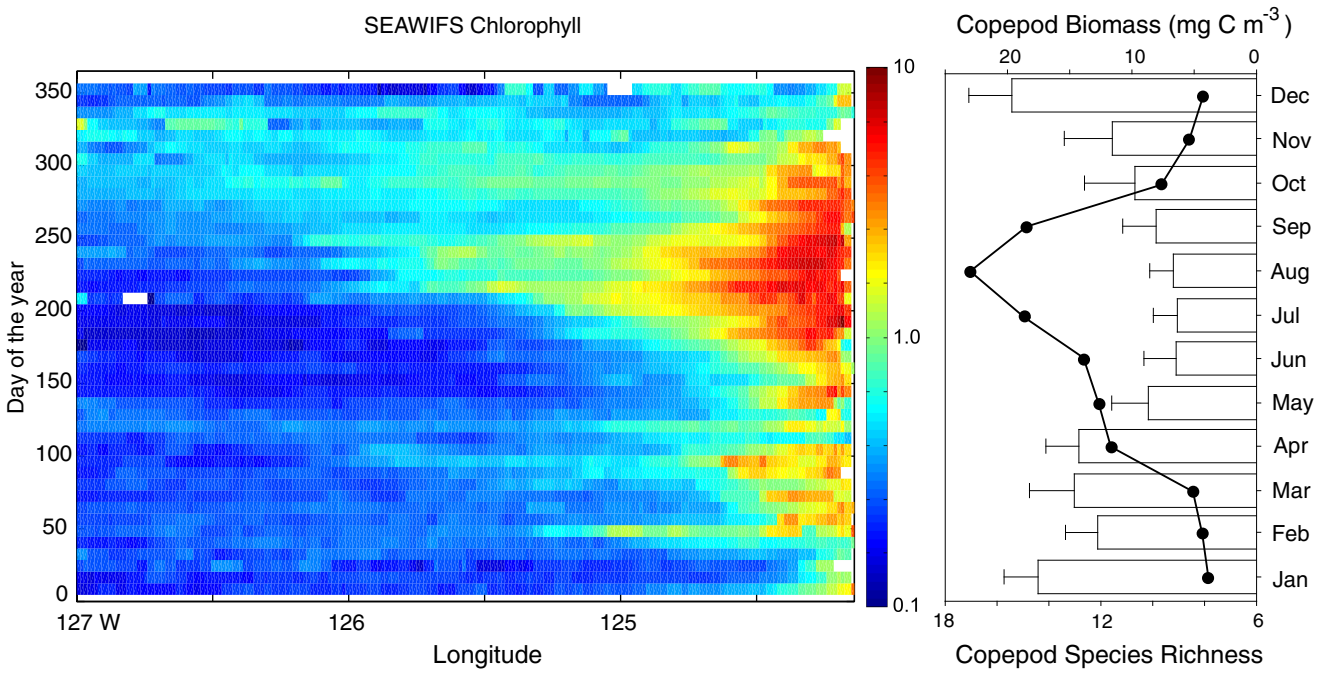
SEAWIFS Chlorophyll
Day of the year
350
300
250
200
150
100
50
0
127 W
126
125
Longitude
10
1.0
0.1
Copepod Biomass (mg C m-3)
20
10
0
Dec
Nov
Oct
Sep
Aug
Jul
Jun
May
Apr
Mar
Feb
Jan
18
12
6
Copepod Species Richness

Figure 17

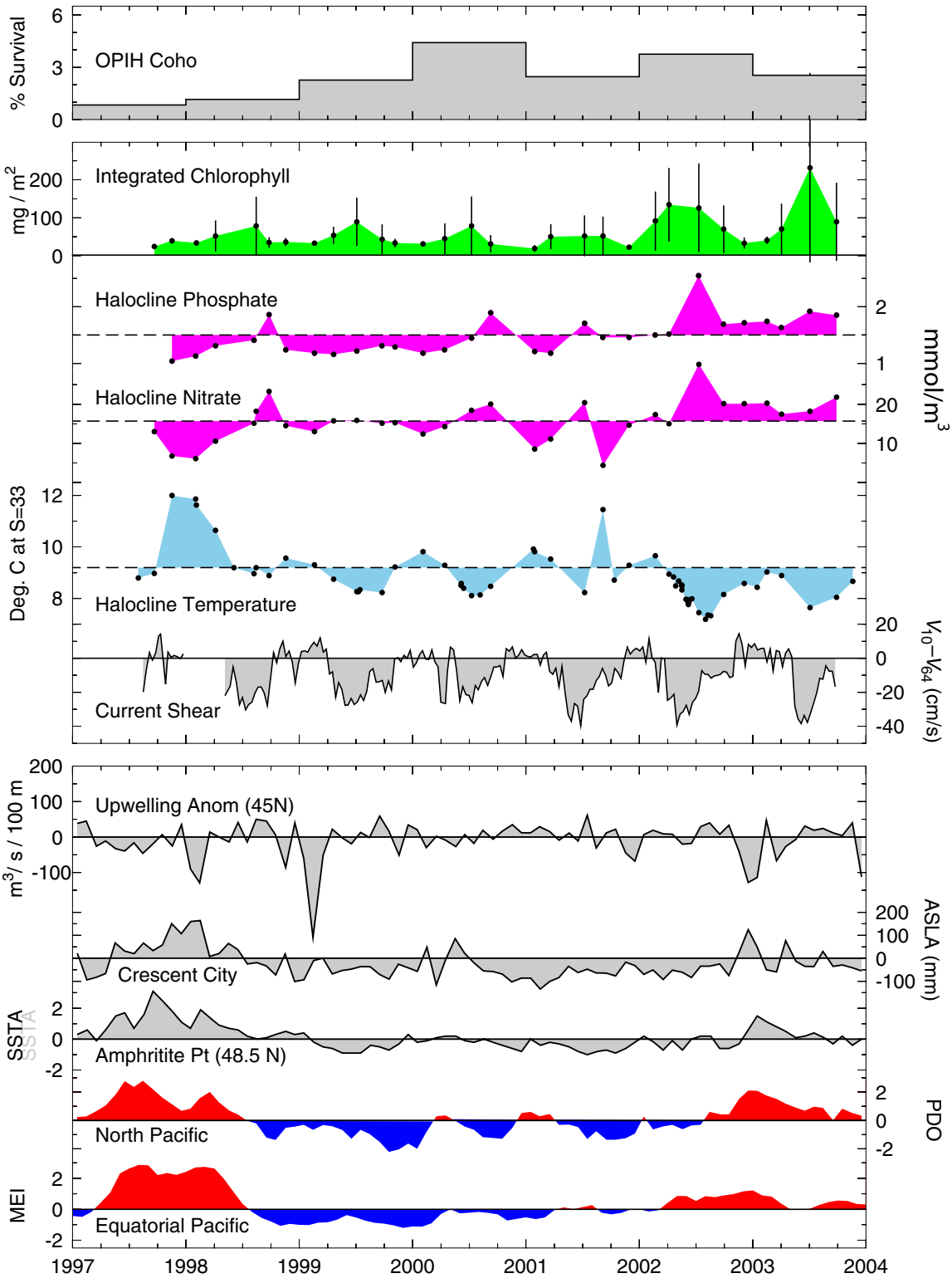
% Survival
OPIH Coho
mg / m2
Integrated Chlorophyll
Halocline Phosphate
Halocline Nitrate
mmol/m3
Deg. C at S=33
Halocline Temperature
Current Shear
V10−V64 (cm/s)
m3/ s / 100 m
Upwelling Anom (45N)
Crescent City
ASLA (mm)
SSTA
Amphritite Pt (48.5 N)
North Pacific
PDO
MEI
Equatorial Pacific
1997
1998
1999
2000
2001
2002
2003
2004

Figure 18

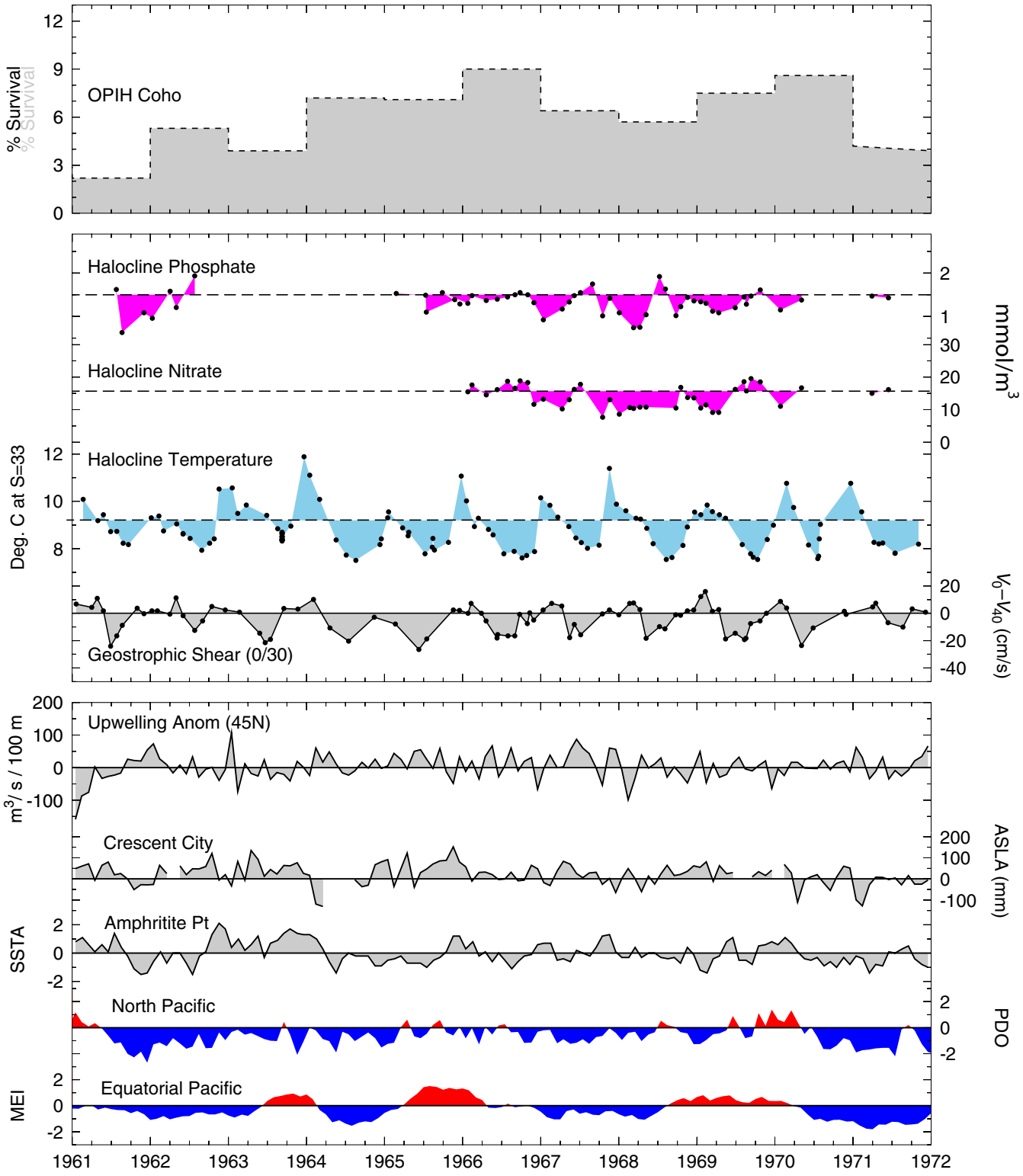
% Survival
OPIH Coho
Halocline Phosphate
Halocline Nitrate
mmol/m3
Halocline Temperature
Deg. C at S=33
Geostrophic Shear (0/30)
V0–V40 (cm/s)
Upwelling Anom (45N)
m3/ s / 100 m
Crescent City
ASLA (mm)
Amphritite Pt
SSTA
North Pacific
PDO
Equatorial Pacific
MEI
1961
1962
1963
1964
1965
1966
1967
1968
1969
1970
1971
1972

Figure 19